Alteration of the Fogera Plain flood regime due to Ribb Dam construction, Upper Blue Nile Basin, Ethiopia

Mulatu, Chalachew A.; Crosato, Alessandra; Langendoen, Eddy J.; Moges, Michael M.; McClain, Michael E.

DOI
10.1080/23249676.2021.1961618

Publication date
2021

Document Version
Final published version

Published in
Journal of Applied Water Engineering and Research

Citation (APA)
Mulatu, C. A., Crosato, A., Langendoen, E. J., Moges, M. M., & McClain, M. E. (2021). Alteration of the Fogera Plain flood regime due to Ribb Dam construction, Upper Blue Nile Basin, Ethiopia. *Journal of Applied Water Engineering and Research*, *10*(3), 175-196. https://doi.org/10.1080/23249676.2021.1961618

Taylor & Francis
Taylor & Francis Group

Journal of Applied Water Engineering and Research

ISSN: (Print) (Online) Journal homepage: https://www.tandfonline.com/loi/tjaw20

Alteration of the Fogera Plain flood regime due to Ribb Dam construction, Upper Blue Nile Basin, Ethiopia

Chalachew A. Mulatu, Alessandra Crosato, Eddy J. Langendoen, Michael M. Moges & Michael E. McClain

To cite this article: Chalachew A. Mulatu, Alessandra Crosato, Eddy J. Langendoen, Michael M. Moges & Michael E. McClain (2021): Alteration of the Fogera Plain flood regime due to Ribb Dam construction, Upper Blue Nile Basin, Ethiopia, Journal of Applied Water Engineering and Research, DOI: 10.1080/23249676.2021.1961618

To link to this article: https://doi.org/10.1080/23249676.2021.1961618

Published online: 06 Aug 2021.

Journal of Applied Water Engineering and Research, 2021
https://doi.org/10.1080/23249676.2021.1961618

Alteration of the Fogera Plain flood regime due to Ribb Dam construction, Upper Blue Nile Basin, Ethiopia

Chalachew A. Mulatu [a,b,c*], Alessandra Crosato [a,b], Eddy J. Langendoen [d], Michael M. Moges [c] and Michael E. McClain [a,b]

[a]*Department of Water Resources and Ecosystems, IHE Delft Institute for Water Education, Delft, The Netherlands;* [b]*Faculty of Civil Engineering and Geosciences, Delft University of Technology, Delft, The Netherlands;* [c]*Faculty of Civil and Water Resources Engineering, Bahir Dar Institute of Technology (BiT), Bahir Dar University, Bahir Dar, Ethiopia;* [d]*Research Hydraulic Engineer, Agricultural Research Service, U.S. Department of Agriculture, Washington, DC, USA*

(*Received 3 February 2021; accepted 23 July 2021*)

The Fogera Plain, Ethiopia, is affected by recurrent flooding of the Ribb and Gumara Rivers. A large dam on the Ribb River is under construction for irrigation, but also to reduce flooding. We investigated the effects of the dam on the flood regime of the floodplain wetlands using a combination of hydrodynamic and a rainfall-runoff models. The model was calibrated based on inundation maps retrieved from Landsat images. Pre- and post-dam model comparison for 10 years shows that the dam will reduce the flooding extent by 11%, as it only regulates 23.8% of the upstream watershed. The flood extent and duration necessary to maintain ecologically significant water depths ($\geq$ 0.5 m) show no notable changes. The developed hydrologic and hydrodynamic models can be used to analyze other dam operation and climate change scenarios even though there are uncertainties related to terrain resolution and analysis of hydrological data.

Keywords: Dam impact study; Blue Nile Basin; Fogera Plain; Ribb River; Gumara River; wetlands ecology

1. Introduction

Flooding is a natural phenomenon that occurs when river channels do not have enough capacity to handle the discharge generated from their watersheds (Leon et al. 2014; Teng et al. 2017). Among the so-called natural disasters, flooding caused more than half of the fatalities (Opperman et al. 2009) and accounts for one-third of economic losses (Pilon 2002). In recent decades, the frequency of floods and associated damage have increased rapidly due to economic activities in fertile flood-prone areas and climate changes (Svetlana et al. 2015). According to the international disaster database report cited by Hu et al. (2019), on average 85 million people were affected per year between 2007 and 2016, with an annual economic loss of 36.7 billion US dollars. It is believed that flood disasters cannot be avoided; however, the associated impacts can be reduced by awareness and preparedness. Floods also provide benefits for the ecology of floodplains, rivers, wetlands, and estuaries (FitzHugh and Vogel 2011). This includes the replenishment of soil nutrients, promoting the upriver migration of fishes for spawning, and support of aquatic habitats.

Dams reduce flooding by attenuating peak discharge (Petts 1980; Kondolf 1997; Petts and Gurnell 2005; Graf 2006; Mei et al. 2017). The immediate hydrological effects are a change in frequency of high and low flows and their time of occurrence, reducing the peak and often increasing the low flows to produce a new hydrograph (Williams and Wolman 1984; Magilligan and Nislow 2005; Graf 2006; Ronco et al. 2010; Grant 2012). These changes affect the flooding extent of downstream floodplains and lower the groundwater table, which may adversely impact habitats of endemic floodplain species (Talukdar and Pal 2019; Li et al. 2020).

Peak discharge attenuation promotes vegetation encroachment and growth on river banks, which controls the river width by reducing bank erosion. Discharge attenuation affects downstream wetlands and agricultural activity (Kondolf 1997) by decreasing lateral connectivity between floodplains and river channels, which is important to maintain wetland habitats in the floodplain (Ward et al. 2002; Talukdar and Pal 2019). The blockage of sediment and debris to the downstream floodplain also affects soil fertility, habitat complexity and reduces food for aquatic species (Qicai 2011).

The replenishment of fertile, clay soils by recurrent flooding of the Ribb and Gumara Rivers makes the vast agricultural land of the Fogera Plain suitable for enhanced agricultural production. However, flooding often results in fatalities and displaced people, which adversely affects the local economy. A dam is under construction in the

*Corresponding author. Email: chalachew1@gmail.com, c.mulatu@un-ihe.org

headwaters of the Ribb River to impound 234 million m^3 of water that will be used to reduce flooding and irrigate 15,000 ha of command area (BRLi and MCE 2010). The construction of the Ribb irrigation system will affect the direct supply of water and nutrients from the river to the wetlands in the Fogera Plain. Hence, the floodplain may face important changes in the near future, which on one hand are expected to improve the local economy and safety, but on the other hand may negatively impact the floodplain ecosystem.

The main objective of this study is to analyze the potential effects of Ribb Dam operation on the river discharge regime and the extent and duration of flooding in the Fogera Plain. It also assesses the potential implications of hydrological alteration on floodplain ecological dynamics. We applied the HEC-HMS (Hydrologic Engineering Center-Hydrologic Modeling System) hydrological model (version 4.3) to determine the discharge time-series of the major rivers entering the Fogera Plain, as the existing discharge measurement stations are unable to gauge the overbank flow, and for the Ribb reservoir flood routing. The model output was used as input for a HEC-RAS 2D (Hydrologic Engineering Center-River Analysis System) hydrodynamic model (version 5.0.7) to compute the pre- and post-dam Fogera Plain flooding extent. Historical inundation maps were retrieved for 01 August 2010 from the spectral difference of the ground objects reflectance values of Landsat satellite images using the cloud-computing-platform of Google Earth Engine to calibrate the hydrodynamic model. Even though the approach in this study does not present a novel understanding of the effect of dams on downstream flooding and ecological changes, it provides important new knowledge to apply specifically in the Upper Blue Nile Basin. Moreover, the approach and findings of the work can be used as a baseline to study similar river basin planning efforts, especially in ungauged and scarcely gauged river basins.

This paper first describes the study area, including the hydrological condition of the major rivers and the status of the Fogera Plain wetlands. It then presents the materials, methods general workflow and model integration (Section 3), including the sources and required input data for the hydrologic, hydrodynamic, and remote sensing methods. Section 4 presents the results, followed by the discussion in Section 5. Finally, Section 6 presents the conclusions and limitations of the study.

2. Study area and data sources

The Fogera Plain is located on the eastern periphery of Lake Tana, the source of the Blue Nile River, Ethiopia. The Ribb and Gumara Rivers are the two major perennial rivers that pass through the Fogera Plain and cause flooding due to their reduced local channel capacity (SMEC 2008b; Dessie et al. 2014; Mulatu et al. 2018). The rivers originate in the Guna Mountains, flow westward receiving additional discharge from tributaries, and finally enter Lake Tana (Figure 1). Sixty-four percent of the Ribb and Gumara watersheds are dominated by cultivation, while 11% of the Gumara and 10% of the Ribb watersheds are covered by shrubs and bushlands. Ungauged watersheds surrounding the Ribb and Gumara Rivers contribute water to the Fogera Plain either by ephemeral tributaries or by overland flow. The central part of the ungauged watershed has an area of 200 km^2 (Figure 1), in which 76% and 10% of the area are dominated by cultivation and farm villages, respectively. Near the Lake Tana shore, the average monthly maximum temperature varies from 17°C to 37°C and from 19°C to 39°C for the Gumara and Ribb watersheds based on data of Woreta and Addis Zemen meteorological stations (1995–2015), respectively. In December, the temperature in the headwaters of the Gumara and Ribb watersheds falls below 0°C (Debre Tabor meteorological station). The Ribb and Gumara watersheds receive an average yearly rainfall of 1300 and 1320 mm, respectively, with higher precipitation in their upper mountainous areas and less near the lake shore. The rainfall is unimodal and 80% falls in the rainy season (June to September).

2.1. *The Ribb River watershed*

The Ribb River has two gauging stations: the Lower and the Upper, which encompass a watershed area of 1501 and 844 km^2, respectively (Figure 1). The watershed elevation varies from 4081 m a.s.l. near the source to 1786 m a.s.l. near Lake Tana. Terrain analysis shows that 18.3%, 42.0% and 49.7% of the watershed area have a slope of less than 10%, between 10% and 20% and greater than 20%, respectively. The river slope is relatively steep (0.3%) near the source and becomes gentle ($\sim$0.037%) in the Fogera Plain. In an attempt to reduce the impacts of recurrent flooding of the lower river reach (downstream of the road connecting the cities of Bahir Dar and Gondar), embankments along the river were constructed (SMEC 2008b; Mulatu et al. 2018). The Ribb Dam is located 3.5 km upstream of the Upper Gauging Station with a watershed area of 715 km^2. Ribb Dam construction was started in 2010. Consequently, the time-series of river discharge after this period may not represent the natural flow as it may be affected by the construction process. The project is not yet operational, as the construction of the irrigation canal system is not complete.

2.2. *The Gumara River watershed*

The Gumara River has one gauging station near the Gumara Bridge, on the road connecting Bahir Dar and Gondar, with a watershed area of 1412 km^2 (Figure 1). The watershed is characterized by undulating topography with an elevation that varies from 3704 m a.s.l. at the source

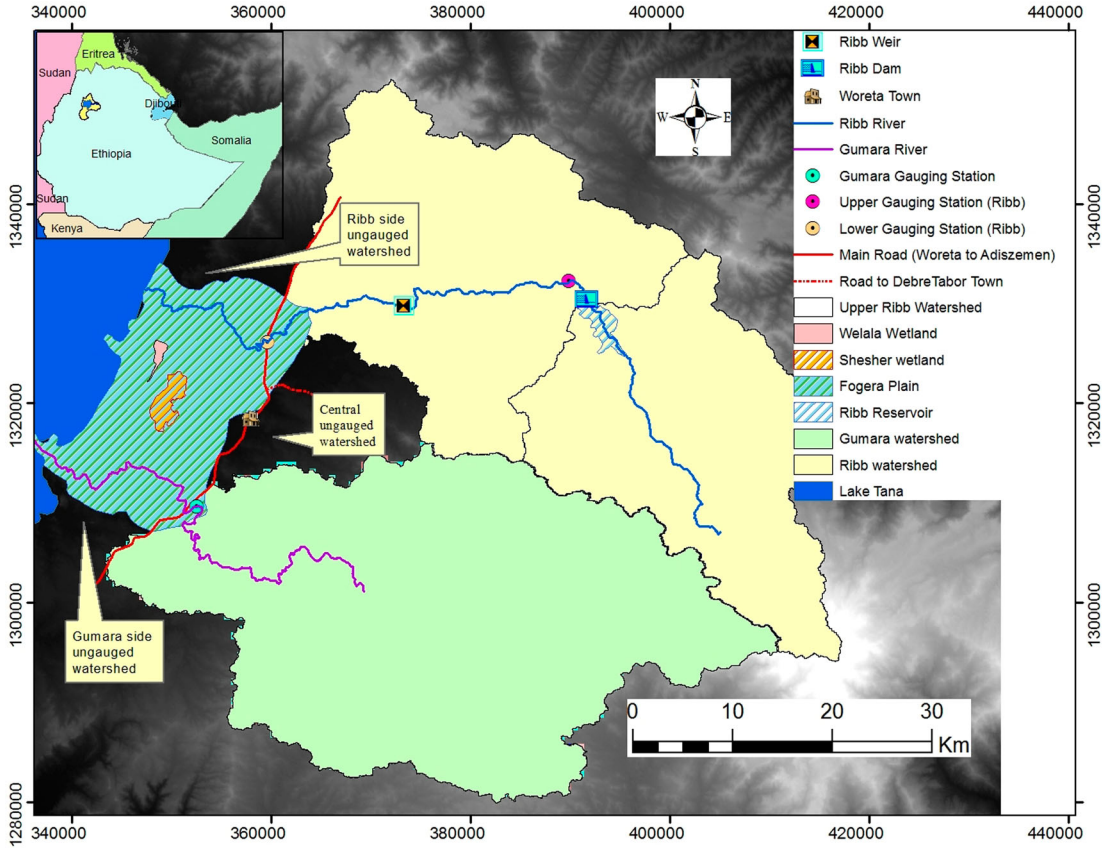

Figure 1. Geographical setting of the Fogera Plain and the Ribb and Gumara watersheds with rivers and wetlands indicated.

to 1786 m a.s.l. near Lake Tana. 25.7% of the watershed area has a slope less than 10%, mainly in the Fogera Plain, while 33.2% of the area has a slope between 10% and 20% and the remaining 41.1% is characterized by steep slopes greater than 20%. Like the Ribb River, the Gumara River reach below the bridge is affected by recurrent flooding (Abate et al. 2015).

2.3. The Fogera Plain

The Fogera Plain experiences recurrent flooding, mainly in August and the beginning of September (SMEC 2008b). Flooding events in 2006 and 2010 were exceptional for their long duration and a high number of fatalities and displaced people, affecting farmlands, houses, health centers, water facilities and other infrastructure (ENTRO 2010). The 2006 flooding displaced more than 30,000 people, killed 45 people, damaged a thousand hectares of agricultural lands, and demolished infrastructure (ENTRO 2010). The average flooding extent of the Fogera Plain was studied by SMEC (2008b) using satellite images of the years from 2001 to 2006 and was estimated to be about 275 km^2 during the month of July. Flooding of the Fogera Plain is mainly caused by: (i) overbank flow from the Ribb and Gumara Rivers due to insufficient channel conveyance capacity (SMEC 2008b; Abate et al. 2015; Mulatu et al. 2018); (ii) direct rainfall and local runoff on the clay soil of the plain in combination with low gradients and poor drainage to the main river systems (Liu et al. 2008; SMEC 2008b); (iii) backwater from Lake Tana due to lake level regulation at its outlet (SMEC 2008b); and (iv) additional water flow to the plain from ungauged watersheds surrounding the Ribb and Gumara Rivers (Figure 1).

Of the 383 km^2 of the Fogera Plain (Figure 1), 288 km^2 are dominated by cultivated land followed by 56.2 km^2 of water bodies and wetlands, 31.1 km^2 of scattered farm villages, and the remaining 7.3 km^2 is shrub, bushlands, forest, and grasslands. Soil texture analyses show that 91% of the plain is dominated by clay with low infiltration rates. The dominant soil type of the two major wetlands (the Welala and the Shesher) is gleysol, characterized by prolonged saturation and a low rate of infiltration.

The wetlands are located in the active flooding zone. They are the spawning and breeding places of locally important fish species (Francis and Aynalem 2007; Mohammed and Mengist 2019), in which Clarias gariepinus and Labeobarbus are the dominant species (Anteneh et al. 2012). These species migrate upriver during the rainy season (July to October) to spawn in the well-oxygenated, clear and fast flowing water, and return to Lake Tana when the flooding recedes (October to December) (Anteneh et al. 2012; Abebe et al. 2020). The wetlands are an attractive

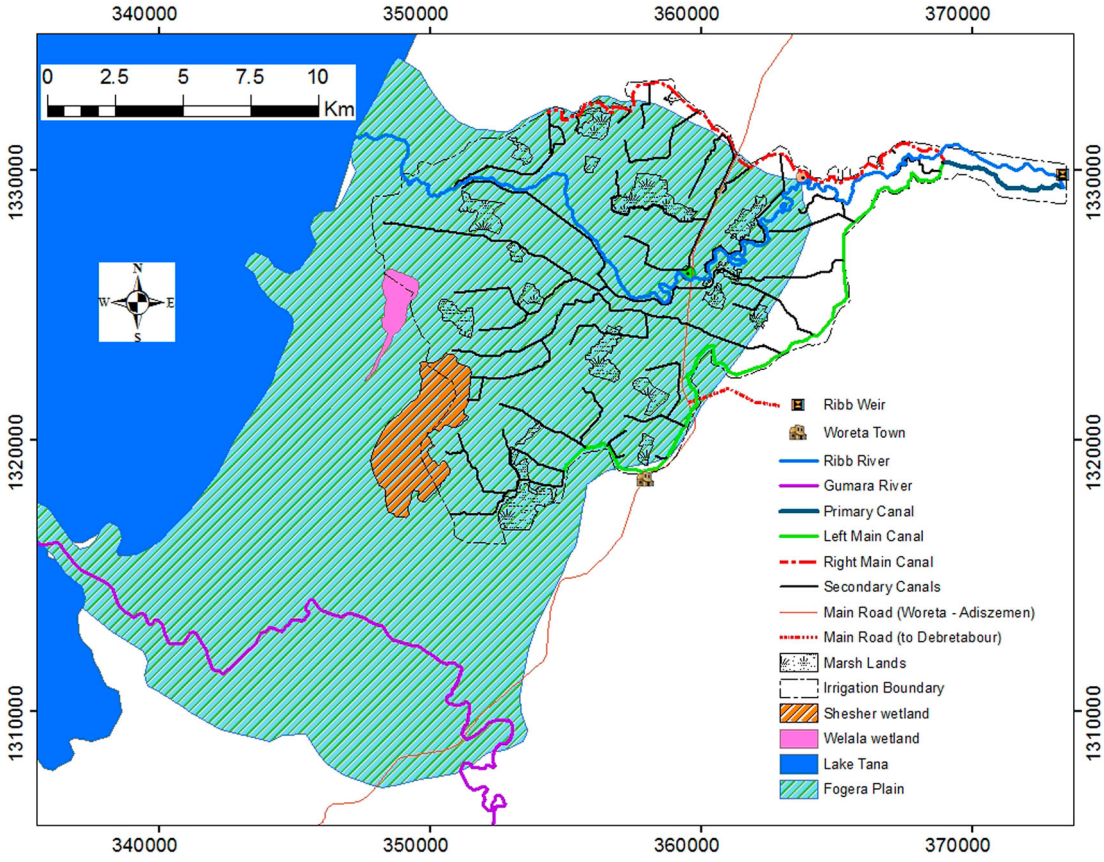

Figure 2. Ribb irrigation boundary with primary, main and secondary canal layouts, and marshlands to be used as a collection chamber for irrigation drainage water (Source: AutoCAD drawing of the feasibility and detail study of Ribb Dam Irrigation system (2010)).

area for birds feeding on fish, insects, cereals, vegetables and fruits (Mitsch 2005; Aynalem 2017). The wetlands provide shelter and roosting places for globally endangered and endemic birds (Mundt 2011; Negash et al. 2011), and serve as an important stopover and breeding place for migratory birds like the Egyptian Goose, Curlew Sandpiper, Common Crane, Black Crowned Crane, and Spur-winged Goose (Francis and Aynalem 2007; Negash et al. 2011; Aynalem 2017).

The wetlands are a source of economic activities like cattle watering and grazing, fishing, farming, and sand mining (Negash et al. 2011; Wondie 2018). In the dry season, water extraction for irrigation and conversion of wetlands to agricultural lands are common practices that have affected both the quantity of water and the biodiversity composition (Wondie 2018; Mohammed and Mengist 2019). Studies by Wondie (2018) and Mohammed and Mengist (2019) indicated that the wetland surface area has been greatly reduced due to intensive agriculture, free grazing, and population density.

The implementation of the Ribb irrigation system will cover a gross area of 16,700 ha, of which 85.7% is in the Fogera Plain located along the Ribb River (Figure 2). The wetlands (including the Welala and Shesher) and the marshlands of the floodplain are planned to serve as a collection chamber/detention basin for the excess irrigation water from the farmlands in the dry season.

2.4. *Data sources*

The data required for the study were obtained from different sources (Table 1). This includes the collection of time-series discharge data of the Ribb and Gumara Rivers and Lake Tana water levels from the Ethiopian Ministry of Water, Irrigation, and Electricity (MoWIE), and rainfall data at the nearby meteorological stations from the Ethiopian National Meteorological Agency (NMA). Literature such as SMEC (2008a), Dessie et al. (2014), Abate et al. (2015), Mulatu et al. (2018), and Mulatu et al. (2020) were reviewed to understand the current state of river discharge, anthropogenic effects, and geometric characteristics. The data needed for the Ribb reservoir flood routing were extracted from the Ribb Dam feasibility study and design documents of WWDSE and TAHAL (2007).

3. Material and methods

This study applied a combination of hydrologic and hydrodynamic numerical models. The integration of the models and the general workflow are shown in Figure 3.

Table 1. Collected data and their sources. TM for Landsat 5 satellite image stands for Thematic Mapper, indicating the type of earth observing instrument mounted on the satellites.

Data type	Data period	Resolution	Source
Digital Elevation Model (DEM)	2014	30 m by 30 m	https://earthexplorer.usgs.gov/
Ribb and Gumara River discharges	2007–2010	Daily	Ministry of Water, Irrigation, and Electricity of Ethiopia (MoWIE)
Ribb and Gumara River cross-sections	–	–	MoWIE (collected during the study and design of Ribb irrigation project)
Lake Tana water level	2007–2019	Daily	MoWIE (Bahir Dar station)
Rainfall at the nearby meteorological stations	2007–2019	Daily	Ethiopian National Meteorological Agency (NMA)
Landsat 5 satellite images (L5-TM)	2010 and 2011	30 m by 30 m	http://landsat.gsfc.nasa.gov/

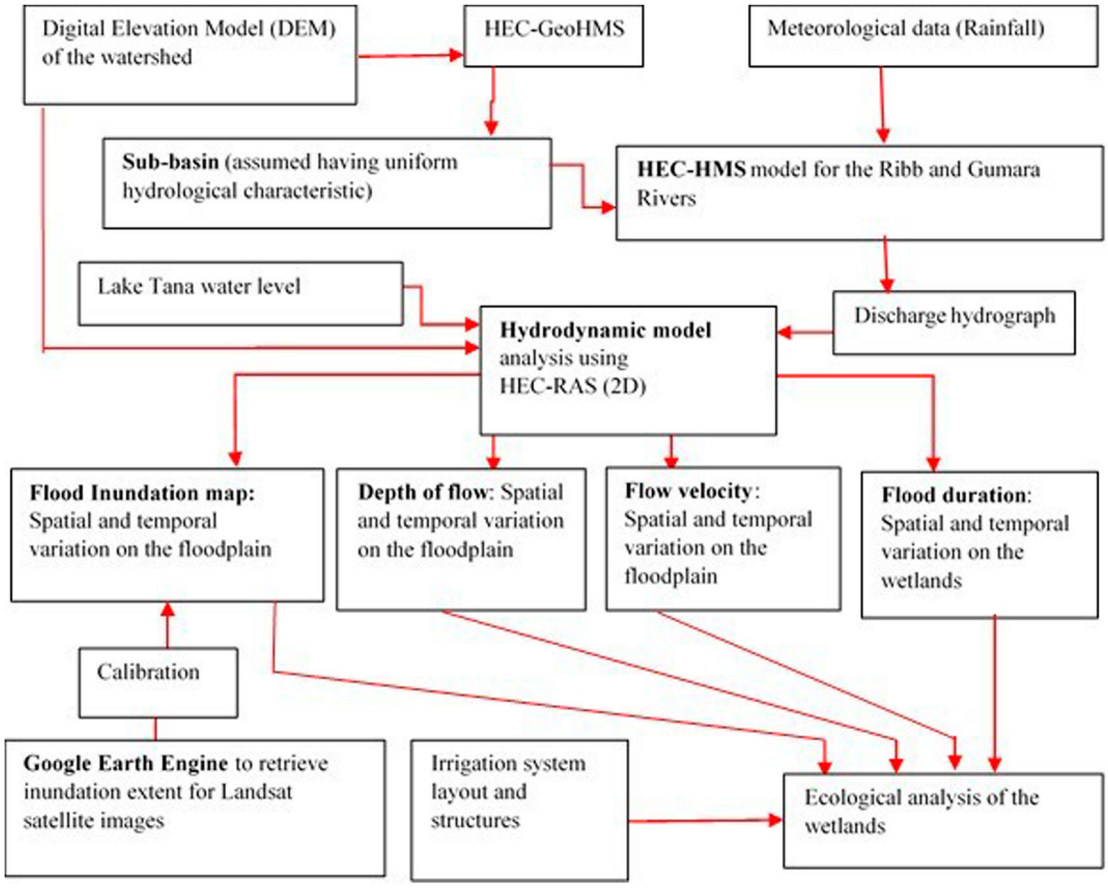

Figure 3. Work flow and model integration.

3.1. Discharge analysis

3.1.1. Pre-dam

The Lower Gauging stations of the Ribb and the Gumara Rivers are located within the floodplain where the peak discharges that cause flooding are not confined by the banks (SMEC 2008b; Dessie et al. 2014; Mulatu et al. 2018). For example, Dessie et al. (2014) indicated a peak flood reduction, relative to the rated discharge, of the Ribb River at the Lower Gauging station up to 71% between December 2011 and December 2012. Therefore, the discharge data of the rivers derived from gauging stations' rating curves cannot be used for flood flow analysis in this study. Instead, a HEC-HMS rainfall-runoff model was developed for the Ribb and Gumara River watersheds to determine the daily time-series discharge data. HEC-HMS is developed by the United States Army Corps of Engineers (USACE) and can simulate the rainfall-runoff process of dendritic watershed systems (Scharffenberg and Fleming 2016). It is selected as it has been successfully applied to simulate both short- and long-term rainfall-runoff events in Ethiopia (Zelelew and

Melesse 2018; Tassew et al. 2019). Moreover, data availability, the ability of the model to operate large tasks, and modeling experience were considered.

Using the Thiessen Polygon (TP) method (e.g. Shaw et al. 2010), the average rainfall over the area (RF_{aerial}) is computed by Equation (1).

$$RF_{aerial} = \sum_{i=1}^{n} \left(\frac{R_i * A_i}{A_t} \right) \quad (1)$$

where R_i is the rainfall at the i-th meteorological station (mm day^{-1}), A_i is the polygon area of the i-th meteorological station (km^2), A_t is the total watershed area (km^2), and n is the number of stations.

The initial (Ia) and constant (Ca) loss method and the Clark Unit Hydrograph (UH) transformation method were selected to compute the rainfall depth and the direct runoff for the watersheds, respectively. These methods are selected based on data availability and used mostly to simulate short-duration events (Jin et al. 2015; Zelelew and Melesse 2018). The Clark UH method requires the time of concentration (T_c, h), which is the maximum travel time in the watershed, and the storage coefficient (Ra) that accounts for the temporary storage of excess precipitation (Feldman 2000). The T_c was estimated using the Kirpich (1940) equation, written as Equation (2). The lag channel routing method, which determines the required time to translate the inflow hydrograph to outflow without attenuation, is selected as it is widely used for the analysis of drainage channels (Scharffenberg and Fleming 2016).

$$T_c = 0.00013 * {L_m}^{0.77} * {S_L}^{-0.385} \quad (2)$$

where L_m is the maximum flow length (ft) and S_L is the channel slope (-).

The HEC-HMS hydrological model was calibrated and validated against the daily time-series discharge data of the Lower Gauging stations for 'dry-years' in which the river discharge does not breach the banks (Table 2). The availability of continuous discharge and rainfall data for the respective hydrological and meteorological stations were also considered.

The model performance was measured using the Nash-Sutcliffe Efficiency (NSE) (Equation (3)) and coefficient of determination (R^2) methods (Equation (4)). Also, the comparison between the simulated and observed volume and peak discharge values and date of occurrences were considered. Watershed (the Ca and Ia loss scale factors, and the Tc and Ra transform methods) and reach (the lag time) parameters were automatically optimized during the calibration process by maximizing the NSE and R^2 values.

$$NSE = 1 - \frac{\sum_{i=1}^{n} (Q_{m,i} - Q_{s,i})^2}{\sum_{i=1}^{n} \left(Q_{m,i} - \overline{Q_m}\right)^2} \quad (3)$$

$$R^2 = \frac{\left[\sum_{i=1}^{n} \left(Q_{m,i} - \overline{Q_m}\right)\left(Q_{s,i} - \overline{Q_s}\right)\right]^2}{\sum_{i=1}^{n} \left(Q_{m,i} - \overline{Q_m}\right)^2 \sum_{i=1}^{n} \left(Q_{s,i} - \overline{Q_s}\right)^2} \quad (4)$$

where $Q_{m,i}$ and $Q_{s,i}$ are the measured and simulated daily discharge values (m^3 s^{-1}), respectively, and $\overline{Q_m}$ and $\overline{Q_s}$ are the measured and simulated average daily discharge values (m^3 s^{-1}), respectively. Model performance can be considered very good, good, satisfactory, and unsatisfactory if R^2 and NSE vary from 0.75 to 1, 0.65 to 0.75, 0.50 to 0.65, and < 0.5, respectively (Moriasi et al. 2007).

The calibrated and validated watershed model for dry-years (Table 2) was run from 2010 to 2019 to generate daily pre-dam river discharge time-series data for the Ribb and Gumara Rivers at their Lower Gauging stations including peak discharge values. Sub-watersheds, which are an important input parameter for the HEC-HMS model (Figure 4) were generated from the DEM of the watershed using HEC-GeoHMS.

The sensitivity of the peak discharge and discharge volume values to the watershed and reach parameters was determined by varying the parameters between -30% and $+30\%$ with respect to the calibrated values. Sensitivity analysis informs how the model output is affected by changing the model simulation parameters (Rauf and Ghumman 2018). Moreover, watershed and reach parameter uncertainty analysis was done using a Monte Carlo analysis of HEC-HMS 4.3 manager for 1000 trials. As described by Oubennaceur et al. (2018) and Shamsudin et al. (2011), this is used to provide an insight into how well the model is calibrated and to identify the possible range of model parameters.

3.1.2. *Post-dam*

The Ribb Reservoir will impound 234 million m^3 of water and inundate an area of 10 km^2 at the Normal Pool Level (NPL) elevation of 1940 m a.s.l. (WWDSE and TAHAL 2007). Sufficient runoff is produced in the rainy season to fill the reservoir fairly quickly; the excess water will pass through the spillway. However, due to the large surface area of the reservoir, the incoming instantaneous peak discharge will be attenuated during outflow.

The HEC-HMS model was developed to determine the time-series outflow discharge using the Modified Puls flood routing method that assumes the reservoir water surface is horizontal. The basic relation for the reservoir flood routing is the continuity of flow, which states that during any time interval the inflow volume is equal to the outflow volume plus/minus change in storage (Fenton 1992; Yang and Cai 2011), given by Equation (5).

$$I_{avg} - O_{avg} = \frac{\Delta S}{\Delta t} \quad (5)$$

where I_{avg} and O_{avg} are the average daily inflow and outflow discharges (m^3 s^{-1}), respectively, over a daily

Table 2. HEC-HMS model calibration and validation periods for the Ribb and Gumara watersheds.

Name of Watershed	Model calibration		Model validation	
	From	To	From	To
Ribb	1-Jun-2007	30-Sep-2007	1-Jun-2008	30-Sep-2008
Gumara	1-Jun-2008	30-Sep-2008	1-Jun-2009	30-Sep-2009

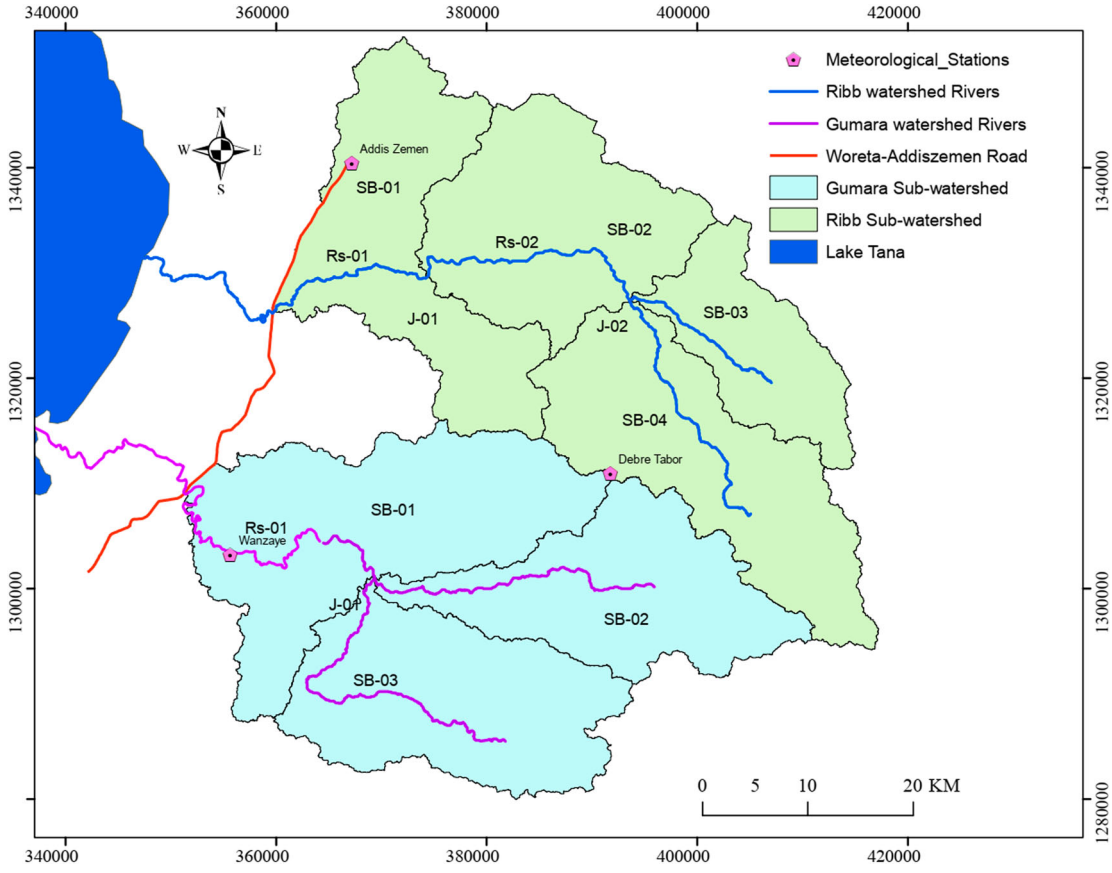

Figure 4. Watersheds for Ribb and Gumara Rivers and reaches (Rs) with river networks with nearby meteorological stations. The abbreviations SB and J stand for sub-watersheds and the junctions of the reaches, respectively.

time step Δt ($=86400$ s), and $\Delta S = (S_{t+1} - S_1)$ is the daily change in storage (m^3). HEC-HMS approximates Equation (5) as Equation (6).

$$\left(\frac{2S_{t+1}}{\Delta t} + O_{t+1}\right) = (I_t + I_{t+1}) + \left(\frac{2S_t}{\Delta t} - O_t\right) \quad (6)$$

where the subscripts t and $t+1$ refer to variable values at the beginning and end of a time step, respectively. To solve for O_{t+1}, we selected the reservoir Elevation-Area-Discharge and the ogee-shaped spillway equations to relate storage to outflow discharge at time $t+1$.

The time-series discharge data of the Ribb River at the dam site, which is one of the inputs for reservoir flood routing, is not available for the study period. Hence, the drainage area proportion method was used to calculate the time-series discharge data at the dam site from the simulated pre-dam values of the Lower Gauging station from 2010 to 2019 (Section 3.1.1), assuming the watershed receives uniform rainfall and generates uniform unit discharge. Other modeling inputs, such as irrigation water requirement, average environmental outflow, elevation-storage characteristics of the reservoir, spillway crest elevation, crest length, and approach depth were obtained from the Ribb Dam feasibility study and design documents of WWDSE and TAHAL (2007). The post-dam discharge at the flood starting point of the Ribb River (2010–2019) was obtained by combining the dam outflow discharge and the discharge from the watershed downstream of the dam.

3.2. *Google Earth Engine application for the pre-dam Fogera Plain flooding*

Applications of remote sensing techniques to determine open water surface area have increased over the last decade (Teng et al. 2017), even though the precise estimation

remains a challenge due to topography, atmosphere, land cover, and sensor limitation (Donchyts et al. 2016). Most of the radiation beyond and inside the near-infrared wavelengths is absorbed by water, enabling the detection of surface water using reflectance spectral index (Donchyts et al. 2016). We used the Modified Normalized Difference Water Index (*MNDWI*) (Equation (7)), which removes the reflectance values of built-up features (Xu 2006; Ji et al. 2009), to determine the open water surface area for the Fogera Plain. The method is applied largely for data-poor regions (Komi et al. 2017; Teng et al. 2017).

$$MNDWI = \frac{Green - SWIR1}{Green + SWIR1} \tag{7}$$

where Green and *SWIR1* represent the surface reflectance values for the green and the shortwave infrared wavelengths, respectively. The *MNDWI* value was calculated using surface reflectance values obtained from Landsat imagery collections within the Google Earth Engine (GEE), and it ranges between -1 and 1.

The determination of open water surface extent by GEE is mainly dependent on the selection of threshold reflectance values (Ji et al. 2009; Donchyts et al. 2016; Tang et al. 2016), which vary with image acquisition time and location (Ji et al. 2009; Feyisa et al. 2014). The Otsu (1979) method was used to determine the threshold reflectance value from the MNDWI histogram for the selected time interval of the study area. For MNDWI values that range from X to Z, the Otsu method divides these values into a water class ($X, \ldots, T$) and a non-water class ($T, \ldots, Z$), where $-1 \le X \le T \le Z \le 1$ and T is the threshold value (Li et al. 2013). The method employs statistical analysis to determine the probability of the pixel being in the water (p_w) and the non-water (p_{nw}) classes. The optimal threshold value is obtained by the in-between class variance of p_w and p_{nw} classes (Li et al. 2013), which is given by Equation (8).

$$T = \arg \max_{X \le T \le Z} \{p_w(M_w - M)^2 + p_{nw}(M_{nw} - M)^2\} \tag{8}$$

where M is the mean of *MNDWI*, and M_w and M_{nw} are the mean *MNDWI* values for the water and non-water classes, respectively.

The methodology was applied to a cloud-free Landsat 5 satellite image for 01 August 2010, as (1) it represents well the flooding period of the study area and (2) the effect of dam construction on the nature of river flow and Fogera Plain flooding is assumed minimum as it was during the starting phase of dam construction. The obtained inundation extent was used as a base-map to calibrate the HEC-RAS 2D hydrodynamic model. Furthermore, the spatial and temporal variation of inundation over the floodplain was studied for the year 2011, in which cloud-free satellite images were available for 26 June, 19 July, 20 August, 21 September, and 23 October.

3.3. *HEC-RAS 2D modeling for the pre- and post-dam Fogera Plain flooding*

For this study, the freely available HEC-RAS 2D (version 5.0.7), developed by the USACE, is selected based on data availability, nature of the problem and study objectives. The model was applied successfully for flood studies (Knebl et al. 2005; Mohammadi et al. 2014; Quirogaa et al. 2016) and the 1D version shows good predictive power if calibrated against inundated area or discharge (Horritt and Bates 2002). Quirogaa et al. (2016) also satisfactorily calibrated the 2D version of the model for the historical inundation area. The model can simulate steady and unsteady flow for supercritical, subcritical, or mixed flow conditions using the 2D Saint Venant or the 2D diffusion wave equations (Brunner 2016). The 2D Saint Venant equations combine the continuity (Equation (9)) and the momentum balance equations in the x (Equation (10)) and y (Equation (11)) directions.

$$\frac{\partial H}{\partial t} + \frac{\partial (hu)}{\partial x} + \frac{\partial (hv)}{\partial y} + q = 0 \tag{9}$$

$$\frac{\partial u}{\partial t} + u\frac{\partial u}{\partial x} + v\frac{\partial u}{\partial y} = -g\frac{\partial H}{\partial x} + v_t\left(\frac{\partial^2 u}{\partial x^2} + \frac{\partial^2 u}{\partial y^2}\right) - c_f u + f v \tag{10}$$

$$\frac{\partial v}{\partial t} + u\frac{\partial v}{\partial x} + v\frac{\partial v}{\partial y} = -g\frac{\partial H}{\partial y} + v_t\left(\frac{\partial^2 v}{\partial x^2} + \frac{\partial^2 v}{\partial y^2}\right) - c_f v - fu \tag{11}$$

where u and v are the depth-averaged velocities in x and y directions ($\mathrm{m\,s^{-1}}$), respectively, q is the source/sink flux term ($\mathrm{m\,s^{-1}}$), H is the water surface elevation (m), h is the flow depth (m), g is the acceleration due to gravity ($\mathrm{m\,s^{-2}}$), v_t is the horizontal eddy viscosity coefficient ($\mathrm{m^2\,s^{-1}}$), c_f is the bottom friction coefficient ($\mathrm{s^{-1}}$), given as $((\eta^2 g|V|)/R^{4/3})$, f is the Coriolis parameter ($\mathrm{s^{-1}}$), $|V|$ is velocity magnitude ($\mathrm{m\,s^{-1}}$), R is the hydraulic radius (m), and η is the Manning's roughness coefficient ($\mathrm{s\,m^{-1/3}}$).

The diffusive wave equations are obtained when assuming the inertial terms are negligible compared to the friction and pressure terms in Equations (10) and (11). The above set of equations is then reduced to Equation (12).

$$\frac{\partial H}{\partial t} + \nabla.\beta\nabla H + q = 0 \tag{12}$$

where $\beta = (-(R(H))^{2/3}/\eta)$ and ∇ is the differential operator $(\partial/\partial x, \partial/\partial y)$.

The stability of the diffusive wave model can be achieved by selecting a time step that satisfies the Courant condition (Equation (13)).

$$C_r = V_w\frac{\Delta t}{\Delta x} \le 2.0 \tag{13}$$

where C_r is the Courant Number with a maximum value for model stability of 2 (-), V_w is the flood wave velocity

($m\,s^{-1}$), Δt is the computational time step (s), and Δx is the average cell size (m). The model allows using varying time steps for the range of Courant Number conditions to give more stability and faster computation time (Brunner 2016).

3.3.1. Model setup

A high-resolution DEM showing the river channel details, one of the main input parameters for the model, was lacking. A separate DEM for the river channels was developed using the reach-averaged river cross-sections and this was combined with the existing DEM using HEC-RAS mapper to produce an improved DEM that includes the river channels. A similar procedure was followed for the major roads. However, a separate DEM was not developed for secondary channels, which will affect the spatial simulation of water entering the floodplain.

Flood inundation analysis using the hydrodynamic model has a certain degree of uncertainty related to the quality of the time-series discharge data, DEM resolution, and model simulation techniques (Oubennaceur et al. 2018; Pinos and Timbe 2019). Sayama et al. (2012) and Komi et al. (2017) indicated that uncertainty analysis that combines hydrologic and hydrodynamic modeling is computationally expensive as it requires the analysis of many uncertain variables. Moreover, our study mainly focuses on the comparison of the pre- and post-dam inundation parameters, for which both models may have similar uncertainty as they are developed for similar boundary conditions and simulation parameters. Hence, this study is limited to the sensitivity analysis of model parameters such as grid spacing, computational time step, and equations to understand the behavioral change of the model output for different values of model parameters.

HEC-RAS allows using large grid spacing as the model extracts detailed elevation values of the cell face like a cross-section from the underlying DEM (Brunner 2016) (see Figure 10(A)). However, model sensitivity was examined for grid spacings of 60, 90, and 120 m. The working domain of the floodplain was defined using the HEC-RAS mapper as a closed polygon to develop the 2D model grids for the specified spacing. Breaklines along the major rivers were included to adjust the cell face, align the mesh, and to have a smooth mesh transition from the rivers to the floodplain. Moreover, the model was simulated for the 2D diffusion wave and 2D Saint Venant equations for comparison of results even though Brunner et al. (2015) and Quirogaa et al. (2016) indicated that the 2D diffusive wave equations are computationally more efficient than the full 2D Saint Venant equations with similar results and greater stability. The model was also simulated for 30 min, 1, and 2 h computational time steps to determine its stability and sensitivity related to inundation extent. The final model simulation parameters were selected based on stability and the required time for model simulation.

Table 3. Manning's roughness coefficient for different land uses.

Land use	Area based on land use (km^2)	Average Manning's η (-)	Source
Cultivated land	297.28	0.04	Chow (1959)
Farm village	24.54	0.1	Rendon et al. (2012)
Forest land	3.64	0.15	Chow (1959)
Grassland	1.01	0.03	Chow (1959)
Shrub and bushland	1.11	0.1	Chow (1959)
Water body	18.33	0.042	Rendon et al. (2012)
Wetland	37.09	0.15	Rendon et al. (2012)

The HEC-RAS 2D model with selected modeling parameters was simulated for the 2010 pre-dam time-series discharge of Ribb and Gumara Rivers, generated by the HEC-HMS model, and using the Lake Tana water level as the upstream and downstream boundary conditions, respectively. The model was calibrated against the flood inundation surface area determined from 01 August 2010 Landsat imagery reflectance values. Manning's roughness coefficient (η) (Table 3) was selected as the calibration parameter and the hydrodynamic model was simulated by changing the average roughness values until the best model prediction was obtained. The performance of the hydrodynamic model to capture the retrieved flood inundation area was analyzed using the measure of fit (Bates and De Roo 2000) given by Equation (14).

$$F = \frac{A_{HEC} \cap A_{GEE}}{A_{HEC} \cup A_{GEE}} * 100 \tag{14}$$

where A_{HEC} and A_{GEE} are the wet areas predicted by HEC-RAS and GEE, respectively, $\cap$ and $\cup$ are the mathematical operators for intersection and union, respectively, and computed using the ArcGIS software. The value of F ranges from 0% to 100% representing no and perfect matches, respectively.

The HEC-RAS model does not explicitly simulate infiltration and evaporation of flooded areas (Brunner 2016). This affects the simulated flooding characteristics of the wetlands and the dam impact on their ecological conditions as flood water cannot recede from such depressions. For this, the rate of seepage and evaporation across the Shesher and Welala wetlands was determined based on literature and generated as a source/sink discharge time-series. The rate of evaporation was equated to the monthly average water surface evaporation of Lake Tana from SMEC (2008a), while the rate of infiltration was taken as $0.5\,mm\,h^{-1}$ based on soil characteristics described by Berhanu et al. (2013). The computed time-series data were

used as an internal boundary condition for model simulation. Note, the discharge contribution of the central ungauged watershed to the Fogera Plain (Figure 1) was not included for the hydrodynamic model simulation as it does not have a defined channel outlet.

3.3.2. *Model application*

The calibrated hydrodynamic model was simulated from 2010 to 2019 for the pre- and post-dam scenarios to determine the inundation extent, water depth and flood duration at the floodplain and the wetlands. For each year, the model simulation period ranged from 01 April to 30 November to study the inundation dynamics. The pre- and post-dam flooding characteristics of the Fogera Plain were determined using ArcGIS 10.5.1 on 01 August of each year for comparison and to determine the effectiveness of the dam to reduce the flooding parameters. The hydrodynamic model was also used to simulate only for the Ribb and the Gumara River discharge time-series to understand the connectivity of the wetlands to these rivers.

3.4. *Effect of the Ribb Dam on the Fogera Plain wetlands*

The pre-dam ecological condition of the Fogera Plain, especially the status of the wetlands, was identified based on the literature review of Negash et al. (2011), Wondie (2018), Mohammed and Mengist (2019), and others. These include the assessment of economic and ecological benefits of the wetlands, the lateral connectivity of the wetlands with the major rivers and Lake Tana, the dominant fish types, and the type and characteristics of the birds as described in Section 2.3. The pre- and post-dam hydrodynamic model simulation results on 01 August of each year were compared for the spatial and temporal flooding extent, water depth, and duration on the floodplain and the wetlands using ArcGIS. The fish migration path (i.e. the lateral connectivity of the wetlands to the major rivers and Lake Tana) was assessed for the threshold water depth equal to or greater than ($\geq$) 0.5 m as suggested by Limbu (2020) and Abdel-Hay et al. (2020) for pond farming of Clarias gariepinus fish. Specifically, the pre- and post-dam flood duration for the water depth of ≥ 0.5 m was developed for the Shesher and Welala wetlands to examine its effect on the spawning and reproduction of the common fish species in Fogera Plain wetlands. Generally, the analysis was used to characterize the ecological effects of the Ribb Dam construction on the aquatic life of the Fogera Plain wetlands.

4. Results

4.1. *Hydrological modeling*

4.1.1. *Model calibration and sensitivity analysis*

Table 4 lists the physical characteristics of the reaches (*Rs*) and sub-watersheds (*SB*) of the Ribb and Gumara watersheds, which were produced using HEC-GeoHMS (Figure 4). The data were used as input for HEC-HMS modeling.

Table 4. Sub-watershed and reach characteristics at the Lower Gauging stations for the Ribb and Gumara watersheds.

Watershed	Sub-watershed/ Reach name	Sub-watershed area (km^2)	Reach length (km)	Time of concentration (h)
Ribb	SB-01	427.42		6.7
	SB-02	404.39		5.73
	SB-03	218.9		4.01
	SB-04	449.87		4.95
	Rs-01	–	20.25	–
	Rs-02	–	28.56	–
Gumara	SB-01	547.82	–	7.73
	SB-02	381.56	–	5.6
	SB-03	422.07	–	7.85
	Rs-01	–	29.62	–

The TP analysis shows that the Ribb watershed surface runoff is mainly dominated by the rainfall measured at Addis Zemen ($A_i = 555\,\text{km}^2$) and Debre Tabor ($A_i = 945\,\text{km}^2$) meteorological stations, while the Gumara watershed runoff is dominated by the rainfall measured at the Debre Tabor ($A_i = 752\,\text{km}^2$) and Wanzaye ($A_i = 599\,\text{km}^2$) meteorological stations.

HEC-HMS model calibration at the Lower Gauging stations shows a good agreement with *NSE* values of 0.7 and 0.9 and R^2 values of 0.71 and 0.82 for the Ribb and Gumara watersheds, respectively. The model captured well the observed peak discharge values, their time of occurrence, the discharge volumes (Table 5), and the general temporal trend of the hydrographs for the Ribb and Gumara Rivers (Figure 5). Similarly, model validation shows a good agreement between discharge volumes and peak values (Table 6). Figure 6 shows the simulated and observed hydrographs for the model validation period.

The model simulation shows that the most sensitive parameter affecting the peak and the volume of discharge values for the Ribb watershed is *Ca,* constant loss, followed by *Ra,* the storage coefficient. Changing the calibrated *Ca* value (Table 7) by -30% and $+30\%$ will decrease and increase the peak discharge by 29.5% and 22.4%, respectively. The average lower and upper bound, and the standard deviation values for the most uncertain parameter for the Ribb sub-watershed (*Ca*) is 0.0013, 1 and 0.2856 mm h^{-1}, respectively, as determined using Monte Carlo analysis of HEC-HMS manager for 1000 trials. However, for the Gumara watershed *Ra* is the most sensitive parameter followed by *Ca*. It was observed that changing *Ra* from the calibrated value by -30% and $+30\%$ will decrease and increase the peak discharge by 9% and 6.7%, respectively. The average

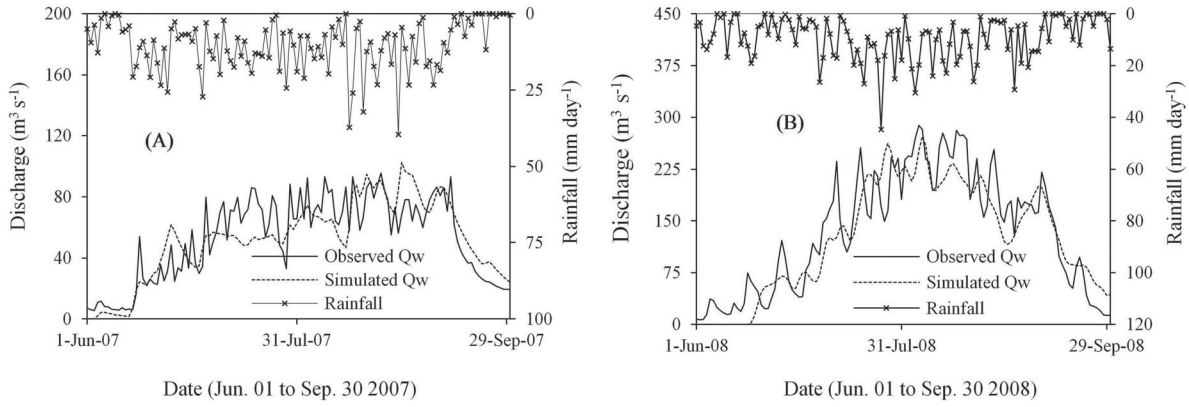

Figure 5. Plots of average rainfall and hydrographs of observed and simulated daily river discharge (Qw) for the model calibration period: (A) Ribb and (B) Gumara watersheds.

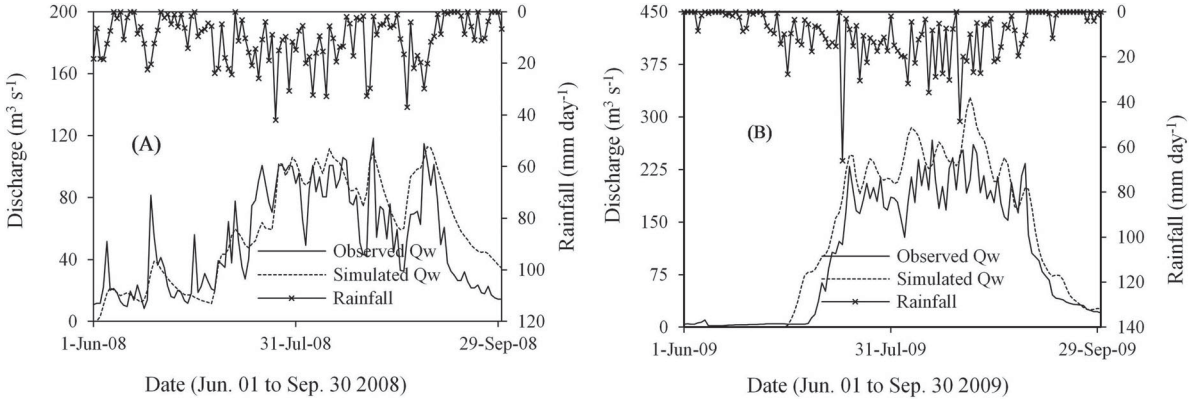

Figure 6. Plots of average rainfall and hydrographs of observed and simulated daily river discharge (Qw) for the model validation period: (A) Ribb and (B) Gumara watersheds.

lower and upper bound, and the standard deviation values for the most uncertain parameter for the Gumara sub-watershed (*Ra*) are 116.94, 283.23 and 48.19 h, respectively.

4.1.2. *Model application for the pre- and post- dam discharge*

The hydrological models of the Ribb and the Gumara watersheds with the calibrated and validated watershed and reach parameters were used to generate the time-series discharge values at the Lower Gauging stations between 2010 and 2019. Model simulation resulted in larger peak discharge values and runoff volumes than those measured. As a result, at the location of the gauging station only part of the total flood flow is measured. For example, Figure 7 shows the comparison between the measured and the simulated discharge values of the 2010 pre-dam scenario. It is found that the model simulation resulted in larger peak discharge values of 214.0 and 393.9 $m^3 s^{-1}$ for the Ribb and

Table 5. Results of HEC-HMS model calibration for the Ribb (01 June to 30 Sep. 2007) and Gumara (01 June to 30 Sep. 2008) watersheds.

Watershed	Parameters	Observed	Simulated	Difference	% Diff	NSE	R^2
Ribb	Volume (million m^3)	369.1	364.3	− 4.8	− 1.3		
	Peak Flow ($m^3 s^{-1}$)	95.7	102.6	6.9	7.2		
	Hydrograph					0.7	0.71
	Time of Peak	24-Aug-07	29-Aug-07				
Gumara	Volume (million m^3)	1047.5	971.9	− 75.6	− 7.2		
	Peak Flow ($m^3 s^{-1}$)	288.2	272	− 16.2	− 5.6		
	Hydrograph					0.9	0.82
	Time of Peak	5-Aug-08	6-Aug-08				

Table 6. Results of HEC-HMS model validation for the Ribb (01 June to 30 Sep. 2008) and Gumara (01 June to 30 Sep. 2009) watersheds.

Watershed	Parameters	Observed	Simulated	Difference	% Diff	NSE	R^2
Ribb	Volume (million m^3)	363.1	412.3	49.3	13.6		
	Peak Flow ($m^3\ s^{-1}$)	118.3	112.7	− 5.6	− 4.7		
	Hydrograph					0.6	0.69
	Time of Peak	23-Aug-08	8-Sep-08				
Gumara	Volume (million m^3)	795.2	995.7	200.6	25.2		
	Peak Flow ($m^3\ s^{-1}$)	266.9	328.1	61.2	22.9		
	Hydrograph					0.8	0.92
	Time of Peak	5-Aug-09	6-Aug-09				

Table 7. Calibrated watershed and reach parameters for the Ribb and Gumara watersheds.

Watershed and Reach parameters	Unit	Watershed/ Reach name	Calibrated parameter for the: Ribb watershed	Gumara watershed
Initial Loss (Ia)	mm	ALL	13.359	71.83
Constant Rate (Ca)	$mm\ h^{-1}$	ALL	0.457735	0.00500435
Time of Concentration (Tc)	h	SB-01	11.925	4.4201
		SB-02	25.141	12.709
		SB-03	5.6773	150.72
		SB-04	10.516	
Storage Coefficient (Ra)	h	SB-01	402.9	164.02
		SB-02	985.02	150.72
		SB-03	164.9	233.54
		SB-04	175.71	

Gumara Rivers, whereas the measured values were 127.7 and 279.1 $m^3\ s^{-1}$, respectively. The difference between the measured and the simulated discharge values represents the ungauged volume of the flood that flows to the Fogera Plain from the Ribb and Gumara Rivers upstream of the gauging stations. Figure 7 shows that the rising limb of the discharge hydrograph for the Ribb and the Gumara Rivers started in June and reached a maximum around the end of August or the start of September.

The HEC-HMS model was also used to simulate the post-dam discharge of the Ribb River at the Lower Gauging station entering the Fogera Plain for use in HEC-RAS 2D. The Ribb Dam reduced the river discharge magnitude on average by 20% and delayed the outflow by one day. For example, the 24 August 2010 peak inflow discharge value of 130.9 $m^3\ s^{-1}$ was reduced by 21% to 103.9 $m^3\ s^{-1}$ and occurred on 25 August 2010.

The post-dam discharge of the Ribb River at the Lower Gauging station, which was obtained by combining the spillover discharge with the discharge generated downstream of the dam, is shown in Figure 8. It shows first a reduction as there is no discharge contribution from the upstream watershed of the dam (i.e. dam filling stage) and then rises sharply and approximates the pre-dam discharge as the water level in the reservoir reaches the spillway crest and spillover starts. Both rivers attain their maximum discharge between the end of August and the start of September.

4.2. *Observed pre-dam Fogera Plain flooding*

The pre-dam inundation area was determined based on Landsat image reflectance values of the ground objects using GEE and found to be 195 km^2 (Figure 9(A)) on 01 August 2010, which covered about 51% of the Fogera Plain. As stated in Section 3.2, the flood map was used as a reference for the calibration of the hydrodynamic model.

The extracted spatial and temporal variations of the open water surface areas for the 2011 rainy season are shown in Figure 9(B–G) to understand the variation throughout the year. At the end of the dry period (June), the Welala wetland is not easily visible (Figure 9(B)). An inundation area of 137 km^2 is observed in the 3rd week of July (Figure 9(C)), which is more concentrated at the upper, roadside part of the floodplain and along the edge of the rivers. The inundation area has increased to 183 km^2 in August (Figure 9(D)) and includes the lower edge of the plain adjacent to Lake Tana. The flooded area is then reduced to 136 km^2 one month later (Figure 9(E)). Inundation areas of 59 and 44 km^2 are observed in September (Figure 9(F)) and October (Figure 9(G)), respectively, and the flooding is mostly limited to depressions, wetlands, and

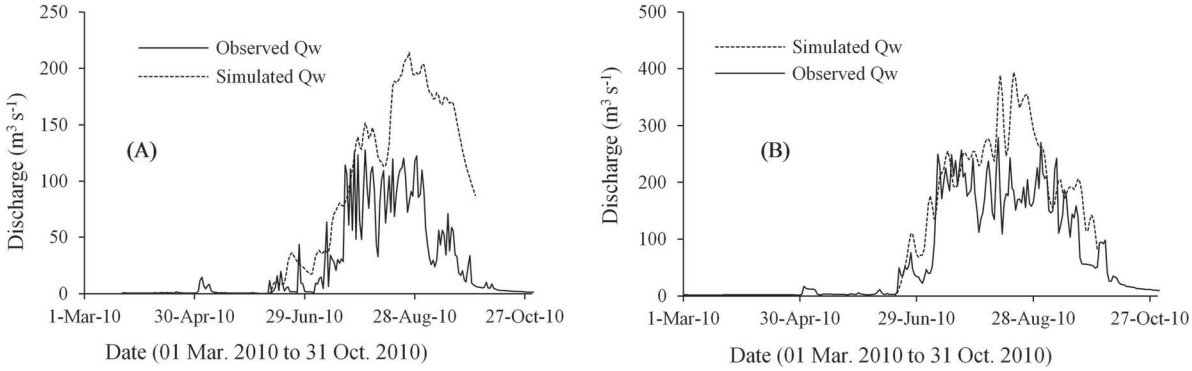

Figure 7. Comparison between simulated and observed daily discharge (Qw) at the Lower Gauging stations for the Ribb (A) and Gumara (B) watersheds. Differences observed and simulated values in peak flows reflect the ungauged portion of the flood flow spilling onto the floodplain upstream of the gauging stations.

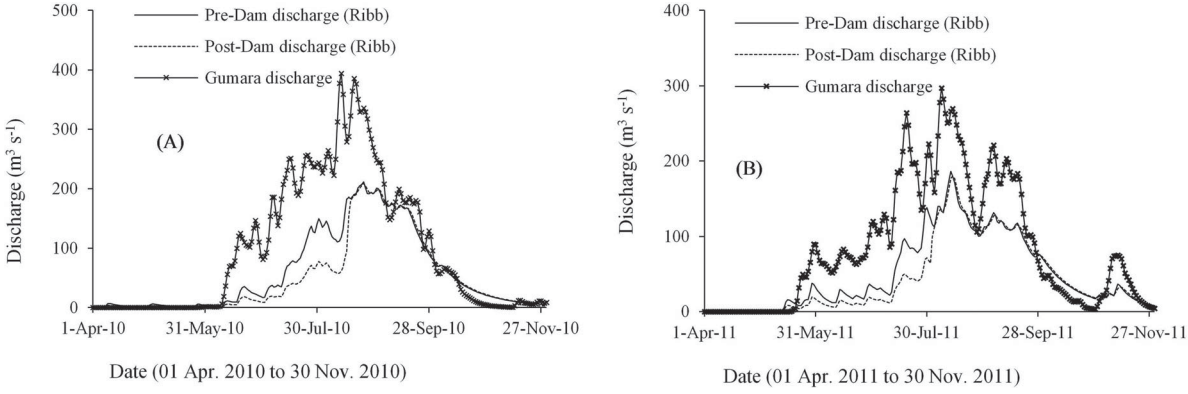

Figure 8. Computed pre- and post-dam discharges for the Ribb and Gumara Rivers at the Lower Gauging stations near the bridges in (A) 2010 and (B) 2011.

along the Lake Tana shoreline. The spatial and temporal flooding variation for the 2011 rainy season is presented here to understand the variation throughout the year.

4.3. *HEC-RAS 2D modeling of the pre- and post-dam flooding*

4.3.1. *Model calibration and sensitivity analysis*

The pre-dam hydrodynamic model calibration began by simulating for the average Manning's η based on land use (Table 3). It resulted in an inundation area of 162 km^2 on 01 August 2010 simulated for 90 m grid spacing and 1 h computational time step. Model simulations using + 50% and + 100% Manning's η resulted in inundation areas of 183 and 188 km^2 on 01 August 2010, respectively. This shows that the model is sensitive to the roughness coefficient with an increased area of inundation for increased roughness. The model performance was assessed using the measure of fit (Equation (14)) and a 46%, 51%, and 52% agreement was obtained between the observed and modeled inundation area for the average, + 50% and + 100% Manning's η modeling scenarios, respectively (Table 8). Manning's η was not increased beyond + 100% as the performance of the model does not show much improvement and, the roughness values will be out of the recommended limits, and it is not reduced from the average value as the model performance becomes poorer. The model simulation for the full 2D Saint Venant equations resulted in a similar flood extent as the diffusion-wave shallow water equations indicating that the flooding extent is controlled by the pressure and bottom friction forces. The model results were found less sensitive to the computational time step, while they are sensitive to grid spacing. Hence, further hydrodynamic model simulations were performed for a 100% increased Manning's η, 2D diffusion-wave equation, 90 m grid spacing and, 1 h computational time step as it shows a better modeling agreement (52%) and it is more stable with less model simulation time. The final model comprises 49,063 cells with an average face length and cell size of 89 m and 7973 m^2, respectively (Figure 10(A)).

4.3.2. *Model simulation for the pre- and post-dam flooding*

Simulation of a calibrated hydrodynamic model for the 2010 post-dam time-series discharge data yields an inundation area of 165 km^2. On average, the Ribb Dam operation

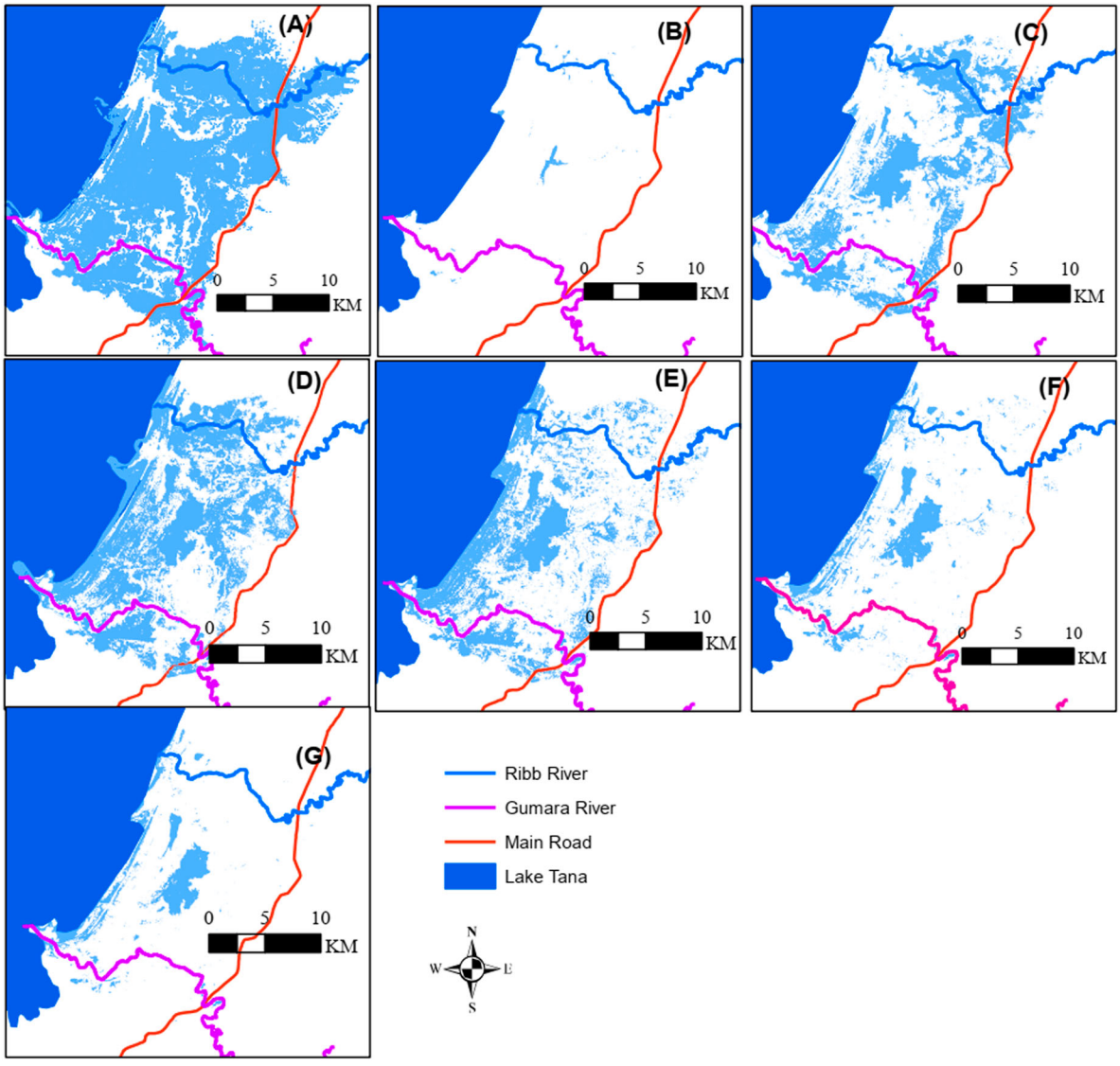

Figure 9. Pre-dam flooding of the Fogera Plain determined using GEE for 01 August 2010 (A). The temporal variation of pre-dam flood inundation for the 2011 rainy season: (B) 26 June, (C) 19 July, (D) 20 August, (E) 21 September, (F) 30 September, and (G) 23 October.

Table 8. Comparison of August 1, 2010 flood inundation extent extracted from Landsat imagery and that simulated by HEC-RAS 2D. Note, the inundation area retrieved from Landsat imagery (AGEE) is 195 km^2.

HEC-RAS 2D model scenarios for Manning's roughness coefficient (η)	Simulated area of inundation (A_{HEC}) (km^2)	$A_{GEE} \cap A_{HEC}$ (km^2)	A_{GEE} U A_{HEC} (km^2)	Measure of Fit, F (%)
Average η	162	107	233	46%
1.5∗Average η	183	125	243	51%
2.0∗ Average η	188	128	245	52%

resulted in an 11% reduction in flooding extent on 01 August compared to the pre-dam scenario (model comparison from 2010 to 2019). Similarly, the average post-dam inundation area for the water depth ≥ 0.5 m was reduced by 19.7%, the pre- and post-dam being 79 and 61.4 km^2, respectively. In both modeling scenarios, the maximum water depth occurred mainly in the rivers, gullies, wetlands, and depression areas and it was concentrated near the lake shore. Figure 10(C) shows the simulated post-dam inundation extent for 01 August 2010, which was reduced by 12.2% compared to the pre-dam scenario (Figure 10(B)), while Figure 10(D) shows the overlay of the pre- and post-dam flooding extents. The post-dam model simulation shows ecologically insignificant velocity change from the pre-dam situation (mainly for fish migration), in both cases, it remains less than 0.6 m s^{-1} and the maximum flow velocity is observed along the rivers and tributaries. For example, on 01 August 2010, the pre- and post-dam flow velocity of the Ribb River near the Lower Gauging station changes from 0.63 to 0.52 m s^{-1},

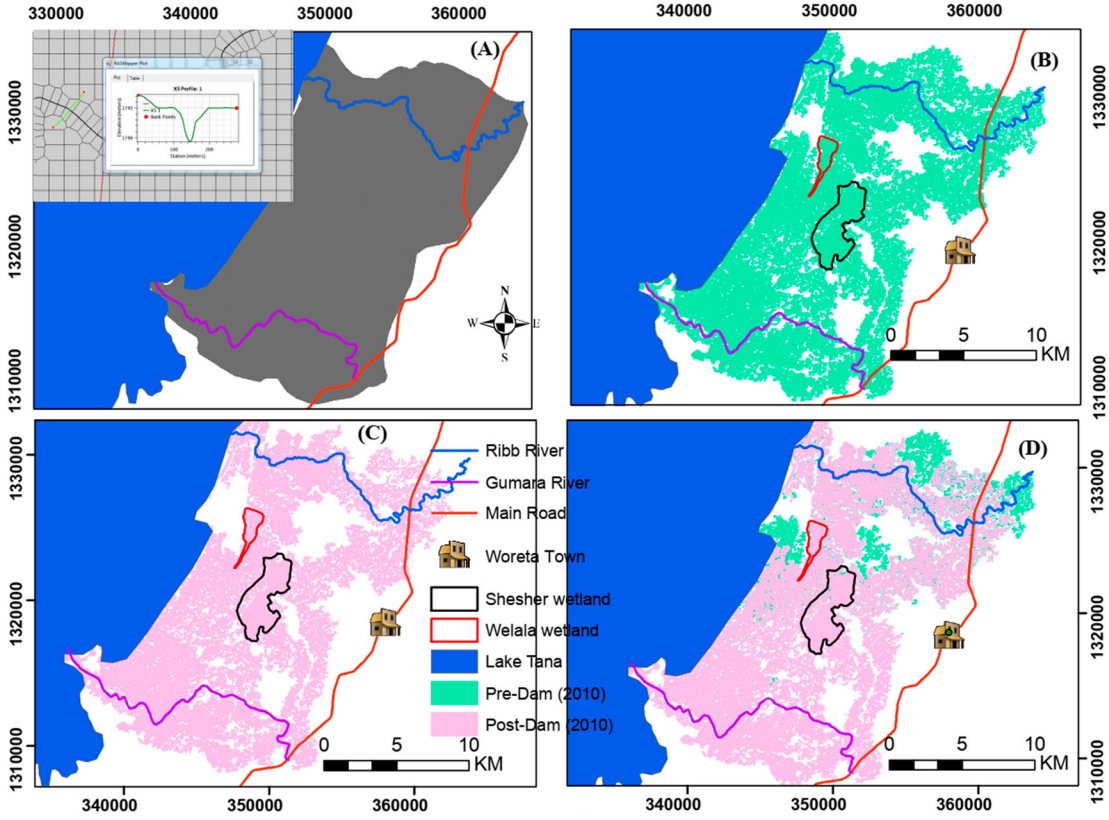

Figure 10. (A) Domain of the HEC-RAS 2D model (mesh extension) with detail of the grid near the Ribb Bridge and profile of the river cross-section at the same location; (B) pre- and (C) post-dam flooding extent of the Fogera Plain determined using HEC-RAS 2D for 01 August 2010; and (D) Overlay of pre- and post-dam flooding extents.

respectively, while the flow velocity of the Gumara River does not show any changes, as it is not affected by regulation. Moreover, the model results represent well the temporal flood variability, which is important to determine maximum flow parameters such as flow velocity and depth.

The pre- and post-dam hydrodynamic model simulation using only the Ribb River discharge data shows that the floodwaters of the river feed both wetlands (Figure 11(A)), though flooding of the Shesher wetland was reduced in the post-dam scenario (Figure 11(B)). The Gumara River floodwaters also supply both wetlands (Figure 11(C)). The post-dam flooding overlay shows that the central part of the Fogera Plain was supplied by both rivers (Figure 11(D)). Dam operation reduces the pre-dam flooding contribution of the Ribb River from 114.2 to 81.8 km^2, while the flooding extent contribution by the Gumara River alone was 119.3 km^2 on 01 August 2010.

The effect on the floodplain of the Ribb River discharge reduction was assessed by comparing the pre- and post-dam discharge hydrographs near the Lower Gauging station with the inflow hydrograph (pre- and post-dam) at the start of the floodplain (Figure 12). It shows that the peak discharge near the Lower Gauging station for the pre- and post-dam condition is similar and did not exceed 110 m^3/s, which is the estimated bankfull discharge at the location as determined by Mulatu et al. (2018). That means the discharge above the bankfull starts to spill to the floodplain before reaching the Lower Gauging station. The pre- and post-dam discharge hydrograph near the Lower Gauging station was obtained from HEC-RAS model simulation.

4.4. *Effect of river regulation on wetland dynamics*

The pre- and post-dam flood inundation extent for a water depth of ≥ 0.5 m (Figure 13), developed for 01 August 2010, was used to study the lateral connectivity of the wetlands to the Ribb and Gumara Rivers and Lake Tana. This helps to determine the possible pathways of fish to the wetlands. It is observed that the post-dam flooded area with water depths ≥ 0.5 m was reduced by 26.8%, the pre- and post-dam flooded areas being 109 and 80 km^2, respectively. The inundation maps were not able to resolve defined channel/pathway connecting the wetlands to the rivers and Lake Tana. Rather, it shows only flows through the floodplain during flooding as indicated in Figure 13(A, B) for the pre- and post-dam modeling scenarios, respectively. The Shesher wetland has a connection with the Gumara River and Lake Tana for the pre- and post-dam

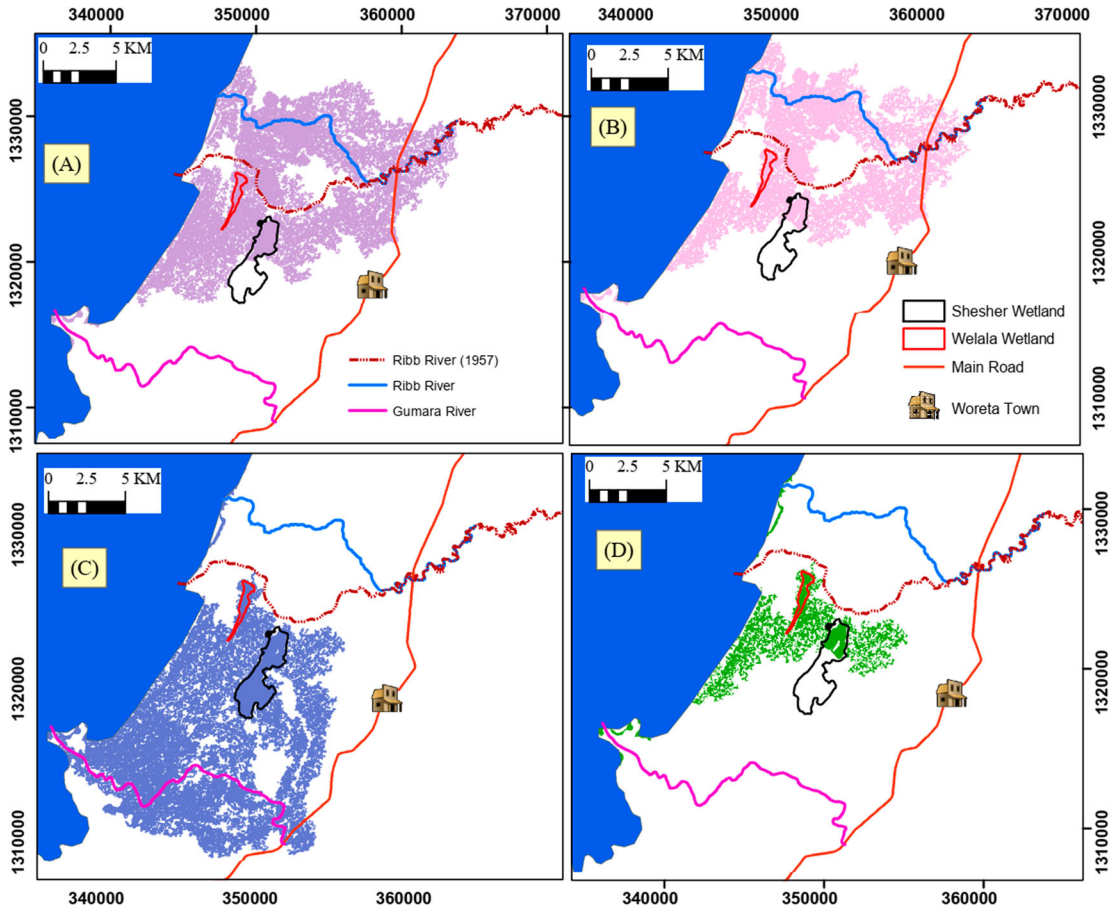

Figure 11. (A) Pre- and (B) post-dam flood inundation by the Ribb River. (C) Flooding by the Gumara River. (D) Area flooded by both rivers on 01 August 2010 for the post-dam scenario.

scenarios. However, the Welala wetland may lose its lateral connectivity to the Ribb River for the post-dam scenario as it receives water only from Lake Tana.

The pre- and post-dam hydrodynamic model analyses for a water depth of ≥ 0.5 m showed that the flood duration for the Shesher and Welala wetlands extends up to four months as shown in Figure 14. The pre- and post-dam flooding extent covers 1.7% and 0.4% of the Shesher wetland for a flood duration of $\geq$ three months, respectively. 17.4% of the pre-dam and 24.4% of the post-dam flooded Shesher wetland area has a flooding duration of ≥ 60 days. Dam operation does not affect the Shesher flooding extent ($\sim 46\%$ of its area) for a flood duration up to 30 days. Hence, the Shesher wetland area that is flooded for more than 30 days is approximately 54% for both pre- and post-dam scenarios. The pre- and post-dam flooding extent of the Welala wetland for a duration of ≥ 90 days covers 3.6% and 5% of the wetland flooded area, respectively. The pre- and post-dam Welala flooding extent for a duration of ≥ 60 days is 93% and 99.2% of the wetland flooded area. Note that the flooded area of the Welala wetland for flood durations less than one month is negligible for both the pre- and post-dam cases. The Ribb Dam operation increases the flood extent for the duration of at least 60 days of the Shesher and Welala wetlands by 7% and 6.2%, respectively, while it shows a negligible effect for flood durations less than 30 days and exceeding 90 days.

5. Discussion

The HEC-HMS hydrological model calibration and validation showed good agreement between the measured and simulated time series discharge values as assessed using NSE and R^2 (Section 4.1.1). However, slight over and under predictions of the low and high flows were observed (Figures 5 and 6), which is a common problem for hydrological models (Zhang and Savenije 2005). Moreover, the results of hydrological modeling may have uncertainties related to model input data, modeling parameters and model selection (Sharafati et al. 2020). River discharge computation based on staff gauge height reading is another source of uncertainty as the rating curves may not be updated regularly for the alluvial river section, which is affected by the river bank and bed morphological adjustments. The model analysis confirms that the most

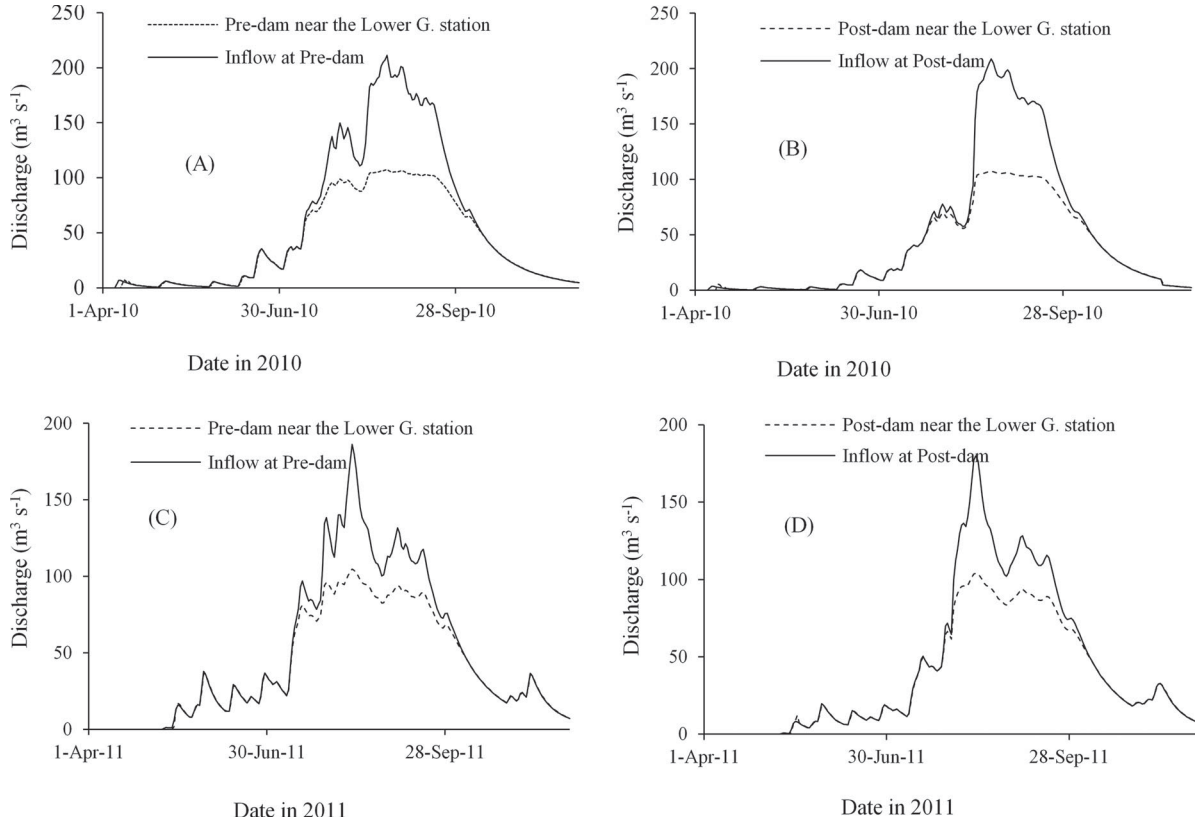

Figure 12. Flow hydrograph at the start of the floodplain and near the downstream gauging station for the pre- and post-dam. (A) and (B) for 2010 and, (C) and (D) for 2011.

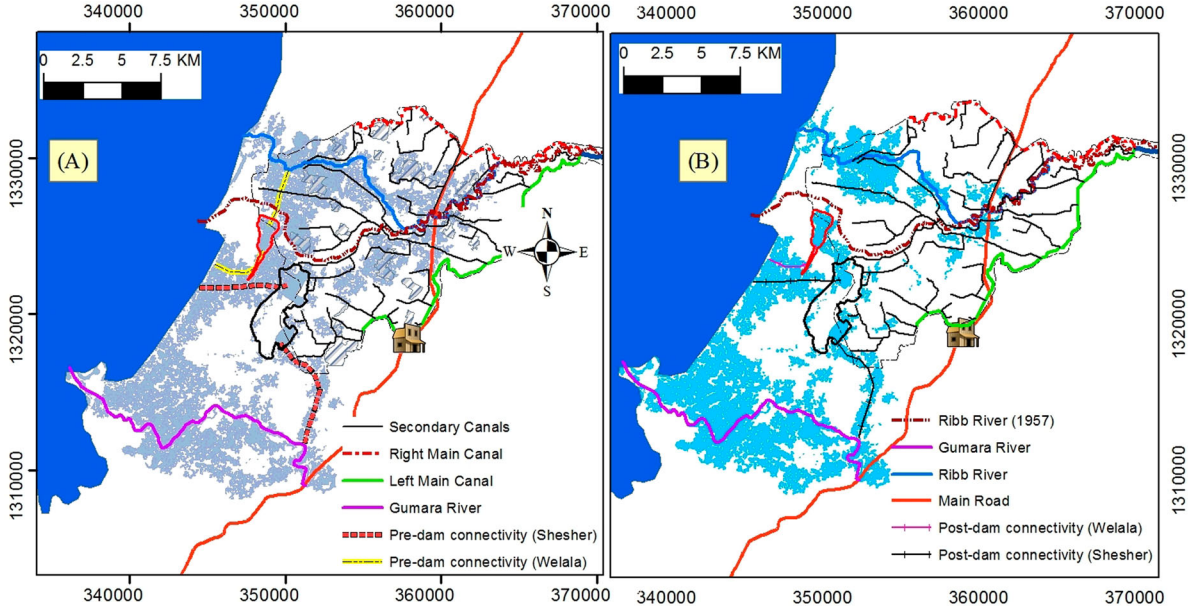

Figure 13. Fogera Plain flooding extent for a water depth equal to or greater than 0.5 m for (A) pre- and (B) post-dam scenarios on 01 August 2010. The solid red polygon delineates the Welala wetland, while the solid black polygon delineates the Shesher wetland.

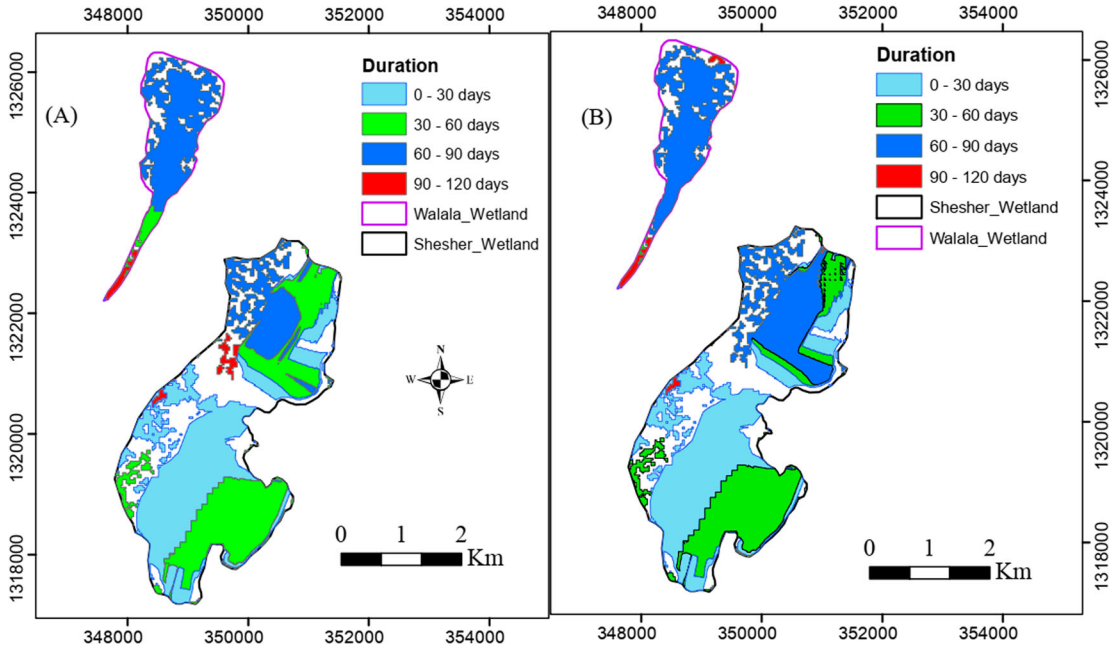

Figure 14. (A) Pre- and (B) post-dam flood duration for the Welala and Shesher wetlands for water depth equal to or greater than 0.5 m for the 2010 rainy season.

uncertain parameters for the Ribb and Gumara watersheds are *Ca* and *Tc*, respectively.

Obtaining historical flooding information is a difficult and uncertain task in data-poor regions, but valuable for the calibration and validation of hydrodynamic models. Due to advances in remote sensing and computer technology, the historical spatial and temporal variations of inundation extent can be obtained by analyzing multiband satellite images using a cloud computing platform to obtain grid-based flooding information. The derived inundation map was used to calibrate the hydrodynamic model and study the pre- and post-dam flooding dynamics of the Fogera Plain. The method was also employed to monitor the spatial and temporal inundation of the floodplain and the wetlands. However, the detection of clear water inundation may be affected by cloud cover, topographically-induced shadows (Donchyts et al. 2016; Teng et al. 2017), and the resolution of the satellite image where mixed land uses in coarse image resolutions affect the reflectance values (Xu 2006).

The developed hydrodynamic model was found more sensitive to the roughness coefficient than the grid spacing. The model simulation for the upper limit of the Manning's η values ($+100\%$ of the average) resulted in a greater inundation extent and a higher water depth compared to the modeling results of the average Manning's η values, which was also noted by Brunner (2016) and Pinos and Timbe (2019). However, it is insensitive to the computational time steps of a similar mesh size. In this study, model simulation for a 90 m grid spacing, 1 h computational time step, and $+100\%$ Manning's η showed an acceptable result with a 52% measure of fit for the inundation extents obtained by remote sensing. However, better model performance was obtained by others, for example (i) Pinos and Timbe (2019) found an agreement ranging from 40.7% to 88.2% for different zones of flooding of the Santa Barbara River basin in the southern part of Ecuador using a flood inundation map produced by a previous HEC-RAS 1D model simulation as a base case; and (ii) Quirogaa et al. (2016) found 72% and 73% inundation agreement between the flooding extent obtained from the moderate resolution imaging spectroradiometer (MODIS) satellite and the HEC-RAS 2D model with varying Manning's η values for Llanos de Moxos floodplain in Bolivian Amazonia. The relatively low model agreement with the inundation extent retrieved using Landsat satellite images may be related to (i) the quality of hydrodynamic model input data including river discharge time-series data, the roughness coefficient, the grid spacing, and the resolution of the underlying topography (DEM) (Oubennaceur et al. 2018; Vojtek et al. 2019); (ii) the accuracy of the method to determine the inundation extent using remote sensing (Donchyts et al. 2016; Teng et al. 2017); (iii) the discharge contribution from the ungauged watersheds by overland flow; and (iv) the direct precipitation on the Fogera Plain. The inability of HEC-RAS 2D version 5.0.7 to consider the effects of evaporation and infiltration was resolved by developing, a time series (negative) discharge that is the sum of evaporation and infiltration for each wetland and imposing it as an internal boundary condition at the lowest-elevation grid cell of the respective wetland.

The Ribb Dam operation was found to attenuate the outflow discharge on average by 20%. A study by Mulatu et al. (2020) using average monthly discharge data showed a similar result in which the dam operation resulted in a reduced wet season peak discharge value by 34%. The hydrologic analysis conducted by WWDSE and TAHAL (2007) for the spillway design also indicated a reduction of maximum outflow discharge by 38%. However, the pre- and post-dam hydrodynamic model simulation showed that the Ribb Dam has a negligible effect on Fogera Plain flooding as it regulates only 23.8% of the total watershed area that contributes flow to the plain. The recent 2019 flooding, which occurred in the middle of August, confirms the ineffectiveness of the dam to reduce flooding. According to regional (Amhara Mass Media Agency) and federal (Ethiopian Broadcast Center) media sources, the flooding was caused by heavy rain in the Ribb watershed, and resulted in three deaths and the inundation of ~4700 houses. During the flooding event, the watershed above the dam was not contributing discharge as it was in the filling stage. This indicates that dam construction at the upper reach of the river system to regulate a small portion of watershed area may have limited influence to attenuate the discharge at the lower reach due to additional discharge from the downstream ungauged watersheds.

The 2010 pre-dam model result showed water depths exceeding 0.5 m cover 55.5% of the inundated area, while this area is reduced by 46.2% for the post-dam scenario. Similarly, the 2010 pre-dam inundated area for water depths exceeding 1 m covers 18.1% of the inundated area and it is reduced to14.2% in the post-dam case. The lag time presented between the maximum Lake Tana water level and the peak discharge of the rivers also helped to reduce the flooding extent. The occurrence of maximum Lake Tana water level in late September resulted in retarded drainage of the plain and an increased flood duration of the wetlands (Figure 9(F)). The post-dam model simulation also showed an insignificant flow velocity reduction compared with the pre-dam case, which is less than 0.6 m s^{-1} in both scenarios.

The Ribb Dam operation will alter the normal river discharge causing reduced and increased wet and dry season values, respectively. The construction of the irrigation system with canals, river bank protection, and water regulatory works may create a barrier that restricts the movement of water and fishes (Figure 2). This may disrupt habitat dynamics, lower the ecosystem productivity, and affect the livelihood of dependent dwellers (Richter et al. 2003). Though the post-dam model simulation shows negligible flood extent reduction of the Fogera Plain, the release of excess water from farmlands in the dry season may shift the seasonal Shesher and Welala wetlands to permanent as they are planned to be used as a detention/collection basin (Figure 2). This could increase fisheries and attract birds and other aquatic communities if the water quality is kept in good condition. Fishing may also be practiced in the Ribb reservoir based on observations from the nearby Koga reservoir.

6. Conclusions

This study assessed the hydrological impact of the Ribb Dam on the Fogera Plain particularly on the flooding dynamics, using the HEC-RAS 2D hydrodynamic model. The results of the model were then used to discuss the alteration of ecologically relevant flow parameters which are vital to study ecological consequences for the Fogera Plain wetlands. The HEC-HMS hydrologic model was used to generate the time-series discharge for the Ribb and Gumara Rivers that flow into the Fogera Plain, including the influence of the Ribb Dam, as the existing measuring stations are unable to gauge the total overbank flow portion. Hydrological model calibration for the Ribb and Gumara watersheds showed an NSE value of 0.7 and 0.9, respectively, while 0.6 and 0.8 for validation.

The application of HEC-HMS for the determination of pre- and post-dam discharge data for the watershed was well understood in the literature. Moreover, the Ribb Dam also controls a small portion of the watershed that drains to the Fogera Plain and the flooding attenuation of the plain was minimal as determined. However, it is important for the region as there is no study done to (1) determine the degree the dam will affect the flooding extent and (2) associate the dam-induced hydrological changes to the ecological consequences that may come due to impoundment at the headwater of the Ribb River. The results of the hydrologic model simulation showed that dam construction at the upper reach of the Ribb River will attenuate the peak discharges, on average by 20%. At the lower gauging station, the natural discharge hydrograph is almost recovered due to flow contributions from the downstream watershed. Moreover, the model can be used to study future watershed development scenarios, including land use and land cover, and climate change.

In this study, we applied the cloud computing platform of GEE to determine the historical inundation maps from the Landsat image reflectance values as historical flood inundation maps are lacking for the region. The mapped flooded areas were then used for the calibration of the hydrodynamic model. The method was found less costly and less time-consuming to map flood inundation with an acceptable level of confidence for data-poor areas.

The results of the hydrodynamic model simulation indicated that the dam does not significantly reduce flooding of the Fogera Plain. The flooding due to Lake Tana backwater dominates in the lake shore area and propagates up the main rivers. The proposed dam operation negligibly affects the lateral connectivity of the Shesher and Welala wetlands (indicative path for fish migration) to the major rivers and Lake Tana. The probable increase in post-dam dry-time

flow to the wetlands from excess irrigation water could further sustain the availability of fish and bird species.

The accuracy of the floodplain terrain representation in the HEC-RAS 2D hydrodynamic model and the boundary conditions may have a significant impact on the results. For this study, a freely available 30 m resolution DEM was sufficient to determine the inundation extent. The post-dam hydrodynamic model simulation showed that the Ribb Dam will reduce the Fogera Plain flooding extent of a water depth exceeding 0.5 m by 26.8%. The results do not show ecologically significant changes in flooding extent and duration of the Shesher and Welala wetlands, which are vital for the survival of the original habitat. However, the developed hydrodynamic model can be used to study different dam operation scenarios to evaluate the change of flooding extent, depth, duration, arrival time, etc. easily at a specific location.

Acknowledgements

The authors acknowledge the Netherlands Fellowship Program (NFP) for the financial support and thank Dr. Seleshi Yalew, Postdoc Researcher at TU Delft, for helping to write the script of Google Earth Engine. We also acknowledge the anonymous reviewers and the editors for their constructive comments.

Disclosure statement

No potential conflict of interest was reported by the author(s).

Notes on contributors

Chalachew A. Mulatu is lecturer in Bahir Dar University, Ethiopia in the Faculty of Civil and Hydraulic Engineering and PhD student in IHE Delft, the Netherlands. His main research focuses on the hydro-morphological and ecological Implications of dam construction on the downstream river systems. The research mainly focused on the Ribb River, Lake Tana Basin, Ethiopia selected as the case study.

Alessandra Crosato is an Associate Professor of River Morphology and River Engineering at IHE Delft, the Netherlands. Her research work mainly deals with the development of bars in river channels and river planimetric changes, as well as floating debris in river channels, for which she carries out laboratory experiments and develops process-based mathematical models.

Eddy J. Langendoen is a Research Hydraulic Engineer with the Watershed Physical Processes Research Unit. His research integrates advances from multiple disciplines covering hydrology, hydraulics, sediment transport mechanics, channel erosion, and bioengineering into a unified, predictive framework to assess the impact of in-stream and riparian zone management on channel morphologic adjustment, with specific emphasis on reducing in-stream sediment loads and improving the ecological integrity of degraded stream systems.

Michael M. Moges is Associate Professor of Hydraulic Engineering at in Bahir Dar University, Ethiopia in the Faculty of Civil and Hydraulic Engineering. Currently, he is working in the Ethiopian Ministry of Water Resources as Senior Ministry advisor. His research focuses are River and Reservoir sedimentation, flow modelling in open channels, modelling of sediment transport in rivers, assessment of climate change impacts at a river basin scale, water resources management and modelling.

Michael E. McClain is Chair Professor of Ecohydrology in IHE Delft, the Netherlands. His research focuses on catchment hydrology and water quality, flow-ecology relationships, environmental flows, and land-water interactions. He routinely advises governmental authorities in a science and management context and leads major research and development projects in Africa and South America.

Data availability statement

Hydrological and meteorological data used for the study were provided by a third party. Direct requests for these materials may be made to the provider.

ORCID

Chalachew A. Mulatu http://orcid.org/0000-0003-2545-0705
Alessandra Crosato http://orcid.org/0000-0001-9531-005X
Eddy J. Langendoen http://orcid.org/0000-0002-2215-4989
Michael M. Moges http://orcid.org/0000-0003-1920-6757
Michael E. McClain http://orcid.org/0000-0003-2956-9818

References

Abate M, Nyssen J, Steenhuis TS, Moges MM, Tilahun SA, Enku T, Adgo E. 2015. Morphological changes of Gumara River channel over 50 years, Upper Blue Nile Basin, Ethiopia. J Hydrol. 525:152–164. doi:10.1016/j.jhydrol.2015.03.044.

Abdel-Hay AHM, Emam W, Omar AA, Eltras WF, Mohamed RA. 2020. The effects of rearing water depths and feed types on the growth performance of African catfish (*Clarias gariepinus*). Aquac Res. 51(2):616–622. doi:10.1111/are.14409.

Abebe WB, Tilahun SA, Moges MM, Wondie A, Derseh MG, Nigatu TA, Mhiret DA, Steenhuis TS, Camp MV, Walraevens K, McClain ME. 2020. Hydrological foundation as a basis for a holistic environmental flow assessment of tropical highland rivers in Ethiopia. Water. 12(2):547. doi:10.3390/w12020547.

Anteneh W, Dejen E, Getahun A. 2012. Shesher and Welala floodplain wetlands (Lake Tana, Ethiopia): are they important breeding habitats for *Clarias gariepinus* and the migratory Labeobarbus fish species? Sci World J. doi:10.1100/2012/298742.

Aynalem S. 2017. Birds of Lake Tana Sub-basin. In: Stave K, Goshu G, Aynalem S, editors. *Social and ecological system dynamics: characteristics, trends, and integration in the Lake Tana Basin, Ethiopia*. Switzerland: Springer International Publishing; p. 179–205.

Bates PD, De Roo APJ. 2000. A simple raster-based model for flood inundation simulation. J Hydrol. 236(1):54–77. doi:10.1016/S0022-1694(00)00278-X.

Berhanu B, Melesse AM, Seleshi Y. 2013. GIS-based hydrological zones and soil geo-database of Ethiopia. Caten. 104:21–31.

BRLi, & MCE. 2010. Pump, drainage schemes at Megech: environmental and social impact assessment of the Ribb Irrigation and Drainage Project.

Brunner GW. 2016. HEC-RAS river analysis system: 2D modeling user's manual. Version 5.0. US Army Corps of Engineers—Hydrologic Engineering Center.

Brunner GW, Piper SS, Jensen MR, Chacon B. 2015. Combined 1D and 2D hydraulic modeling within HEC-RAS. Paper presented at the World Environmental and Water Resources Congress.

Chow VT. 1959. *Open-channel hydraulics: civil engineering series*. New York: McGraw-Hill.

Dessie M, Verhoest NE, Admasu T, Pauwels VR, Poesen J, Adgo E, Deckers J, Nyssen J. 2014. Effects of the floodplain on river discharge into Lake Tana (Ethiopia). J Hydrol. 519:699–710. doi:10.1016/j.jhydrol.2014.08.007.

Donchyts G, Schellekens J, Winsemius H, Eisemann E, van de Giesen N. 2016. A 30 m resolution surface water mask including estimation of positional and thematic differences using landsat 8, srtm and openstreetmap: a case study in the Murray-Darling Basin, Australia. Remote Sens. 8(5):386. doi:10.3390/rs8050386.

ENTRO. 2010. *Flood risk mapping consultancy for pilot areas in Ethiopia. Final report to the Eastern Nile Technical Regional Office (ENTRO)*. Addis Ababa: ENTRO.

Feldman AD. 2000. Hydrologic modeling system HEC-HMS: technical reference manual. US Army Corps of Engineers, Hydrologic Engineering Center.

Fenton JD. 1992. Reservoir routing. Hydrol Sci J. 37(3):233–246.

Feyisa GL, Meilby H, Fensholt R, Proud SR. 2014. Automated Water Extraction Index: a new technique for surface water mapping using Landsat imagery. Remote Sens Environ. 140:23–35. doi:10.1016/j.rse.2013.08.029.

FitzHugh TW, Vogel RM. 2011. The impact of dams on flood flows in the United States. River Res Appl. 27(10):1192–1215. doi:10.1002/rra.1417.

Francis I, Aynalem S. 2007. *Bird surveys around Bahir Dar-Lake Tana IBA, Ethiopia. Report of RSPB Scotland*. Aberdeen: Addis Ababa University, Ethiopia.

Graf WL. 2006. Downstream hydrologic and geomorphic effects of large dams on American rivers. Geomorphology. 79(3):336–360. doi:10.1016/j.geomorph.2006.06.022.

Grant GE. 2012. The geomorphic response of Gravel Bed Rivers to dams: perspectives and prospects. In: Church M, Biron PM, Roy AG, editors. *Gravel-bed rivers: processes, tools, environments*. Chichester: John Wiley & Sons, Ltd; p. 165–181.

Horritt M, Bates P. 2002. Evaluation of 1D and 2D numerical models for predicting river flood inundation. J Hydrol. 268(1-4):87–99. doi:10.1016/S0022-1694(02)00121-X.

Hu X, Pant R, Hall JW, Surminski S, Huang J. 2019. Multi-Scale Assessment of the economic impacts of flooding: evidence from firm to macro-level analysis in the Chinese manufacturing sector. Sustainability. 11(7):1933. doi:10.3390/su11071933.

Ji L, Zhang L, Wylie B. 2009. Analysis of dynamic thresholds for the normalized difference water index. Photogramm Eng Remote Sens. 75(11):1307–1317.

Jin H, Liang R, Wang Y, Tumula P. 2015. Flood-runoff in semi-arid and sub-humid regions, a case study: a simulation of Jianghe watershed in northern China. Water. 7(9):5155–5172. doi:10.3390/w7095155.

Kirpich Z. 1940. Time of concentration of small agricultural watersheds. Civil Eng. 10(6):362.

Knebl M, Yang Z-L, Hutchison K, Maidment DR. 2005. Regional scale flood modeling using NEXRAD rainfall, GIS, and HEC-HMS/RAS: a case study for the San Antonio River Basin Summer 2002 storm event. J Environ Manag. 75(4):325–336. doi:10.1016/j.jenvman.2004.11.024.

Komi K, Neal J, Trigg MA, Diekkrüger B. 2017. Modelling of flood hazard extent in data sparse areas: a case study of the Oti River basin, West Africa. J Hydrol. 10:122–132. doi:10.1016/j.ejrh.2017.03.001.

Kondolf GM. 1997. PROFILE: hungry water: effects of dams and gravel mining on river channels. Environ Manag. 7(4):303–325.

Leon AS, Kanashiro EA, Valverde R, Sridhar V. 2014. Dynamic framework for intelligent control of river flooding: case study. J Water Resour Plan Manag. 140(2):258–268. doi:10.1061/(ASCE)WR.1943-5452.0000260.

Li W, Du Z, Ling F, Zhou D, Wang H, Gui Y, Sun B, Zhang X. 2013. A comparison of land surface water mapping using the normalized difference water index from TM, ETM + and ALI. Remote Sens. 5(11):5530–5549. doi:10.3390/rs5115530.

Li F-F, Liu C-M, Wu Z-G, Qiu J. 2020. Balancing ecological requirements and power generation in reservoir operation in fish spawning seasons. J Water Resour Plan Manag. 146(9):04020074. doi:10.1061/(ASCE)WR.1943-5452.0001277.

Limbu SM. 2020. The effects of on-farm produced feeds on growth, survival, yield and feed cost of juvenile African sharptooth catfish (*Clarias gariepinus*). Aquac Fish. 5(1):58–64.

Liu BM, Collick AS, Zeleke G, Adgo E, Easton ZM, Steenhuis TS. 2008. Rainfall-discharge relationships for a monsoonal climate in the Ethiopian highlands. Hydrol Process Int J. 22(7):1059–1067. doi:10.1002/hyp.7022.

Magilligan FJ, Nislow KH. 2005. Changes in hydrologic regime by dams. Geomorphology. 71(1):61–78. doi:10.1016/j.geomorph.2004.08.017.

Mei X, Van Gelder P, Dai Z, Tang Z. 2017. Impact of dams on flood occurrence of selected rivers in the United States. Front Earth Sci. 11(2):268–282. doi:10.1007/s11707-016-0592-1.

Mitsch WJ. 2005. Invitational at the Olentangy River Wetland Research Park. Wetl Creation Restor Conserv State Sci. 24:243–251.

Mohammadi S, Nazariha M, Mehrdadi N. 2014. Flood damage estimate (quantity), using HEC-FDA model. case study: the Neka river. Procedia Eng. 70:1173–1182. doi:10.1016/j.proeng.2014.02.130.

Mohammed I, Mengist M. 2019. Status, threats and management of wetlands in the lake Tana sub-basin: a review. J Agric Environ Sci. 3(2):23–45.

Moriasi DN, Arnold JG, Van Liew MW, Bingner RL, Harmel RD, Veith TL. 2007. Model evaluation guidelines for systematic quantification of accuracy in watershed simulations. Trans ASABE. 50(3):885–900.

Mulatu CA, Crosato A, Moges MM, Langendoen EJ, McClain M. 2018. Morphodynamic trends of the Ribb River, Ethiopia, prior to dam construction. Geosciences. 8:255. doi:10.3390/geosciences8070255.

Mulatu CA, Crosato A, Moges MM, Langendoen EJ, McClain M. 2020. Long-term effects of dam operations for water supply to irrigation on downstream river reaches. The case of the Ribb River, Ethiopia. Int J River Basin Manag. doi:10.1080/15715124.2020.1750421.

Mundt F. 2011. Wetlands around Lake Tana: a landscape and avifaunistic study [M.Sc.]. Universitat Greifswald, Germany.

Negash A, Eshete D, Jacobus V. 2011. Assessment of the ecological status and threats of Welala and Shesher Wetlands, Lake Tana sub-basin (Ethiopia). J Water Resourc Protect. 2011. doi:10.4236/jwarp.2011.37064.

Opperman JJ, Galloway GE, Fargione J, Mount JF, Richter BD, Secchi S. 2009. Sustainable floodplains through large-scale

reconnection to rivers. Science. 326(5959):1487–1488. doi:10.1126/science.1178256.
Otsu N. 1979. A threshold selection method from gray-level histograms. IEEE Trans Syst Man Cybern. 9(1):62–66. doi:10.1109/TSMC.1979.4310076.
Oubennaceur K, Chokmani K, Nastev M, Tanguy M, Raymond S. 2018. Uncertainty analysis of a two-dimensional hydraulic model. Water. 10(3):272. doi:10.3390/w10030272.
Petts GE. 1980. Long-term consequences of upstream impoundment. Environ Conserv. 7(4):325–332.
Petts GE, Gurnell AM. 2005. Dams and geomorphology: research progress and future directions. Geomorphology. 71(1):27–47. doi:10.1016/j.geomorph.2004.02.015.
Pilon PJ. 2002. Guidelines for reducing flood losses. United Nations International Strategy for Disaster Reduction (UNISDR).
Pinos J, Timbe L. 2019. Performance assessment of two-dimensional hydraulic models for generation of flood inundation maps in mountain river basins. Water Sci Eng. 12(1):11–18. doi:10.1016/j.wse.2019.03.001.
Qicai L. 2011. Influence of dams on river ecosystem and its countermeasures. J Water Resourc Protect. doi:10.4236/jwarp.2011.31007.
Quirogaa VM, Kurea S, Udoa K, Manoa A. 2016. Application of 2D numerical simulation for the analysis of the February 2014 Bolivian Amazonia flood: application of the new HEC-RAS version 5. Ribagua. 3(1):25–33. doi:10.1016/j.riba.2015.12.001.
Rauf A-U, Ghumman AR. 2018. Impact assessment of rainfall-runoff simulations on the flow duration curve of the Upper Indus River—a comparison of data-driven and hydrologic models. Water. 10(7):876. doi:10.3390/w10070876.
Rendon SH, Ashworth CE, Smith SJ. 2012. *Dam-breach analysis and flood-inundation mapping for lakes Ellsworth and Lawtonka near Lawton*. Oklahoma: US Department of Interior, US Geological Survey.
Richter BD, Mathews R, Harrison DL, Wigington R. 2003. Ecologically sustainable water management: managing river flows for ecological integrity. Ecol Appl. 13(1):206–224.
Ronco P, Fasolato G, Nones M, Di Silvio G. 2010. Morphological effects of damming on lower Zambezi River. Geomorphology. 115(1):43–55. doi:10.1016/j.geomorph.2009.09.029.
Sayama T, Ozawa G, Kawakami T, Nabesaka S, Fukami K. 2012. Rainfall–runoff–inundation analysis of the 2010 Pakistan flood in the Kabul River basin. Hydrol Sci J. 57(2):298–312. doi:10.1080/02626667.2011.644245.
Scharffenberg WA, Fleming MJ. 2016. Hydrologic modeling system HEC-HMS: user's manual. US Army Corps of Engineers, Hydrologic Engineering Center.
Shamsudin S, Dan'azumi S, Ab Rahman A. 2011. Uncertainty analysis of HEC-HMS model parameters using Monte Carlo simulation. Int J Model Simul. 31(4):279–286. doi:10.2316/Journal.20.2011.4.205-5487.
Sharafati A, Khazaei MR, Nashwan MS, Al-Ansari N, Yaseen ZM, Shahid S. 2020. Assessing the uncertainty associated with flood features due to variability of rainfall and hydrological parameters. Adv Civil Eng. 2020. doi:10.1155/2020/7948902.
Shaw EM, Beven KJ, Chappell NA, Lamb R. 2010. *Hydrology in practice*. London: CRC Press.
SMEC. 2008a. Hydrological study of the Tana-Beles Sub-basin: Main Report. (5089018). Australia: Snowy Mountains Engineering Corporation (SMEC) International Pty Ltd.
SMEC. 2008b. Hydrological study of the Tana-Beles Sub-basin: Surface water investigation. Australia: Snowy Mountains Engineering Corporation (SMEC) International Pty Ltd.
Svetlana D, Radovan D, Ján D. 2015. The economic impact of floods and their importance in different regions of the world with emphasis on Europe. Proc Econ Financ. 34:649–655. doi:10.1016/S2212-5671(15)01681-0.
Talukdar S, Pal S. 2019. Effects of damming on the hydrological regime of Punarbhaba river basin wetlands. Ecol Eng. 135:61–74. doi:10.1016/j.ecoleng.2019.05.014.
Tang Z, Li Y, Gu Y, Jiang W, Xue Y, Hu Q, LaGrange T, Bishop A, Drahota J, Li R. 2016. Assessing Nebraska playa wetland inundation status during 1985–2015 using Landsat data and Google Earth engine. Environ Monit Assess. 188(12):654. doi:10.1007/s10661-016-5664-x.
Tassew BG, Belete MA, Miegel K. 2019. Application of HEC-HMS model for flow simulation in the Lake Tana Basin: the case of Gilgel Abay Catchment, Upper Blue Nile Basin, Ethiopia. Hydrology. 6(1):21. doi:10.3390/hydrology6010021.
Teng J, Jakeman AJ, Vaze J, Croke BF, Dutta D, Kim S. 2017. Flood inundation modelling: A review of methods, recent advances and uncertainty analysis. Environ Model Softw. 90:201–216. doi:10.1016/j.envsoft.2017.01.006.
Vojtek M, Petroselli A, Vojteková J, Asgharinia S. 2019. Flood inundation mapping in small and ungauged basins: sensitivity analysis using the EBA4SUB and HEC-RAS modeling approach. Hydrol Res. doi:10.2166/nh.2019.163.
Ward J, Tockner K, Arscott DB, Claret C. 2002. Riverine landscape diversity. Freshw Biol. 47(4):517–539. doi:10.1046/j.1365-2427.2002.00893.x.
Williams GP, Wolman MG. 1984. *Downstream effects of dams on alluvial rivers*. Washington (DC): U.S. Government Printing Office.
Wondie A. 2018. Ecological conditions and ecosystem services of wetlands in the Lake Tana area, Ethiopia. Ecohydrol Hydrobiol. 18(2):231–244. doi:10.1016/j.ecohyd.2018.02.002.
WWDSE & TAHAL. 2007. Ribb Dam Hydrological Study (Final Report). Addis Ababa: Water Works Design and Supervision Enterprise (WWDSE) and TAHAL Consulting Engineers Ltd.
Xu H. 2006. Modification of normalised difference water index (NDWI) to enhance open water features in remotely sensed imagery. Int J Remote Sens. 27(14):3025–3033. doi:10.1080/01431160600589179.
Yang Y-CE, Cai X. 2011. Reservoir reoperation for fish ecosystem restoration using daily inflows—case study of Lake Shelbyville. J Water Resour Plan Manag. 137(6):470–480.
Zelelew D, Melesse A. 2018. Applicability of a spatially semi-distributed hydrological model for watershed scale runoff estimation in Northwest Ethiopia. Water. 10(7):923. doi:10.3390/w10070923.
Zhang G, Savenije H. 2005. Rainfall-runoff modelling in a catchment with a complex groundwater flow system: application of the representative elementary watershed (REW) approach. Hydrol Earth Syst Sci. 9:243–261. doi:10.5194/hess-9-243-2005.